JGR Atmospheres

RESEARCH ARTICLE
10.1029/2022JD037135

# Convective Impact on the Global Lower Stratospheric Water Vapor Budget

**Rei Ueyama[1], Mark Schoeberl[2], Eric Jensen[3], Leonhard Pfister[1], Mijeong Park[4], and Ju-Mee Ryoo[1,2]**

[1]NASA Ames Research Center, Moffett Field, CA, USA, [2]Science and Technology Corporation, Columbia, MD, USA, [3]NOAA Chemical Sciences Laboratory, Boulder, CO, USA, [4]National Center for Atmospheric Research, Boulder, CO, USA

**Key Points:**

- Convection moistens the global lower stratosphere by 0.3 ppmv with interannual variations of up to 0.1 ppmv in winter and summer 2006–2016
- Convection moistens the lower stratosphere via the detrainment of saturated air and ice into the tropical uppermost troposphere
- In the absence of cloud-top mixing, overshooting convection has a relatively small effect on global lower stratospheric water vapor

**Correspondence to:**
R. Ueyama,
rei.ueyama@nasa.gov

**Citation:**
Ueyama, R., Schoeberl, M., Jensen, E., Pfister, L., Park, M., & Ryoo, J.-M. (2023). Convective impact on the global lower stratospheric water vapor budget. *Journal of Geophysical Research: Atmospheres*, *128*, e2022JD037135. https://doi.org/10.1029/2022JD037135

Received 17 MAY 2022
Accepted 2 MAR 2023

**Abstract** Water vapor in the stratosphere is primarily controlled by temperatures in the tropical upper troposphere and lower stratosphere. However, the direct impact of deep convection on the global lower stratospheric water vapor budget is still an actively debated issue. Two complementary modeling approaches are used to investigate the convective impact in boreal winter and summer. Convective influence is diagnosed by tracing trajectories through convective cloud top altitude fields derived from global rainfall and brightness temperature data. Backward trajectory model simulations coupled with a detailed treatment of cloud microphysical processes indicate that convection moistens the global lower stratosphere by approximately 0.3 ppmv in boreal winter and summer 2010. The diurnal peak in convection is responsible for about half of the total convective moistening during winter and nearly all of the convective moistening during summer. Deep convective clouds overshooting the tropopause have relatively minor effect on global lower stratospheric water vapor. A forward trajectory model coupled with a simplified cloud module is used to estimate the relative magnitude of the interannual variability of the convective impact. Combining the results from the two models, we find that the convective impact on the global lower stratospheric water vapor during 2006–2016 is approximately 0.3 ppmv with year-to-year variations of up to 0.1 ppmv. An important mechanism of convective hydration of the lower stratosphere is via the detrainment of saturated air and ice into the tropical uppermost troposphere and the subsequent upward transport of some of these moist air parcels across relatively warm and subsaturated tropopause.

**Plain Language Summary** Stratosphere is extremely dry, but small changes in the humidity of the stratosphere can have a big impact on Earth's climate. Water vapor in the stratosphere is primarily determined by temperatures in the tropical upper atmosphere (between the tropospheric and stratospheric layers), but deep convective clouds that rapidly transport humid air up to this region could potentially influence stratospheric water vapor as well. This study uses two complementary modeling approaches to estimate the overall impact of deep convection on global stratospheric humidity. We find that convection moistens the lower stratosphere by about 10% in boreal winters and summers with smaller (by about a third) year-to-year variations during the 2006–2016 period. The daytime peak in convection is responsible for about half of the total convective moistening during boreal winter and nearly all of the convective moistening during boreal summer. Deep convective cloud tops that penetrate into the lower stratosphere have a relatively small effect on stratospheric water vapor. Convection moistens the lower stratosphere by transporting humid air laden with numerous ice crystals to the tropical uppermost troposphere, just below the stratosphere. Some of this humid air subsequently ascends into the stratosphere and ultimately increases the humidity of the lower stratosphere.

## 1. Introduction

Water vapor is an important greenhouse gas and exerts significant influence on the chemistry and radiative balance of the atmosphere (e.g., Anderson et al., 2012; Forster & Shine, 1999, 2002; Solomon et al., 2010). Tropospheric water vapor, for instance, amplifies the direct warming from carbon dioxide via a strong positive feedback mechanism (Schneider et al., 1999; Sherwood et al., 2010). Brewer (1949) hypothesized that the dryness of the stratosphere could be explained by the existence of a global circulation in which air enters the stratosphere through the cold tropical tropopause, where it is dehydrated to the ice saturation level, moves poleward, and descends back down to the troposphere in the extratropics. This large-scale circulation in the stratosphere is known as the Brewer-Dobson circulation (BDC). Yulaeva et al. (1994) later interpreted the relationship between low-latitude and high-latitude temperature annual cycles observed in the lower stratosphere as a result

of variations in the strength of the wave-driven BDC. The annual cycle in tropical tropopause temperature, with a minimum in boreal winter and a maximum in boreal summer, produces a "tape recorder" signal in time-height section of zonal-mean water vapor mixing ratios as seen by satellites (Fueglistaler et al., 2005; Mote et al., 1996; Schoeberl et al., 2008). These and other studies (see Fueglistaler et al., 2009 and references therein) highlight the importance of the strength of the tropical upwelling in the BDC in modulating the cold-point tropical tropopause temperature (Holton et al., 1995), which then controls the stratospheric water vapor budget as described further below.

Despite its very low concentration, stratospheric water vapor affects the chemistry (Anderson et al., 2012; Dvortsov & Solomon, 2001; Kiehl & Solomon, 1986), radiative forcing (Forster & Shine, 1999; Li & Newman, 2020; Solomon et al., 2010), and atmospheric circulation (Maycock et al., 2013). It also produces various feedbacks on the climate system (Banerjee et al., 2019; Dessler et al., 2013; Huang et al., 2020). Because of its significant role on climate, long-term observations of stratospheric water vapor have been made using balloons (Hurst et al., 2016) and various satellite instruments such as Aura Microwave Limb Sounder (MLS; Livesey et al., 2020). These measurements have been useful for monitoring long-term changes and variability in stratospheric humidity, and for investigating processes that influence stratospheric water vapor.

As noted earlier, it is generally well understood that the stratospheric water vapor budget is, to first order, controlled by the slow large-scale ascent through the cold tropical tropopause (Fueglistaler et al., 2005; Gettelman et al., 2002; Hatsushika & Yamazaki, 2003; Holton & Gettelman, 2001; Mote et al., 1996; Randel & Jensen, 2013; Randel & Park, 2019). Processes associated with atmospheric waves and convection also play a role in the dehydration of air entering the stratosphere through the tropical tropopause layer (TTL). These include dehydration driven by the cooling phase of gravity, Kelvin and Rossby waves (Boehm & Verlinde, 2000; Chang & L'Ecuyer, 2020; Dinh et al., 2016; Fujiwara et al., 2009; Garrett et al., 2004; Immler et al., 2008; Jensen & Pfister, 2004; J.-E. Kim et al., 2016; Potter & Holton, 1995; Reinares Martinez et al., 2021; Schoeberl et al., 2015, 2016; Virts et al., 2010) and by the adiabatic cooling of air within deep convective overshooting cloud tops (Danielsen, 1982; Garrett et al., 2004, 2006; Gasparini et al., 2019; Hartmann et al., 2001; J. Kim et al., 2018; Potter & Holton, 1995; Robinson & Sherwood, 2006; Sherwood & Dessler, 2000; Sherwood et al., 2003). Additionally, cloud (microphysical, dynamical, and radiative) processes and the direct injection of water vapor and ice by deep convection can increase stratospheric water vapor (Corti et al., 2008; Danielsen, 1983; Dauhut et al., 2018; Hassim & Lane, 2010; Jensen & Pfister, 2004; Kelly et al., 1993; Kritz et al., 1993; Lee et al., 2019; Nielsen et al., 2007; Pfister et al., 1993; Schoeberl et al., 2014, 2016, 2018; Ueyama et al., 2015, 2018, 2020; Wang, 2003).

The climatological mean distribution of lower stratospheric (83 hPa) water vapor obtained from the Aura MLS measurements in boreal winter and summer is shown in Figure 1. In boreal winter, there is a distinct minimum in water vapor mixing ratios over the western tropical Pacific, roughly coincident with the region of minimum tropopause temperatures. In contrast, there is no obvious relationship between lower stratospheric water vapor and temperature fields in boreal summer. Rather, enhanced water vapor over the Asian summer monsoon region appears to be collocated with a region of deep convective activity. The high water vapor mixing ratios in the extratropics are due to the transport of moist air associated with methane photolysis at higher altitudes in the stratosphere (Wofsy et al., 1972).

The role of deep convection as a source of stratospheric water vapor has been explored over decades (Adler & Mack, 1986; Avery et al., 2017; Corti et al., 2008; Danielsen, 1983; Dessler et al., 2016; Kelly et al., 1993; Nielsen et al., 2007; Schoeberl et al., 2014, 2018, 2019; Smith et al., 2017; Wang et al., 2019). There is evidence of the direct injection of ice crystals (and subsequent sublimation) in the lowermost stratosphere by deep convection overshooting the tropopause, such as in the tropics (Corti et al., 2008) and over the midlatitude summer monsoon regions (Lee et al., 2019; Schwartz et al., 2013; Smith et al., 2017). Several studies using storm-resolving models have indicated that tropopause-overshooting convection can hydrate the lower stratosphere (Dauhut et al., 2018; Dauhut & Hohenegger, 2022; Hassim & Lane, 2010; Wang, 2003), but the impact of overshooting convection on the global stratospheric water vapor budget based on observations is less clear (e.g., Jensen et al., 2020). In the current climate, only a small fraction of convective systems penetrates high enough into the stratosphere to have a significant impact (Liu & Zipser, 2005).

The detrainment of ice and its subsequent sublimation in the tropical uppermost troposphere could potentially hydrate the lower stratosphere, if the detrained ice and the convectively influenced air parcel do not ascend through highly supersaturated (with respect to ice) air. Trajectory studies indicate that most parcels entering

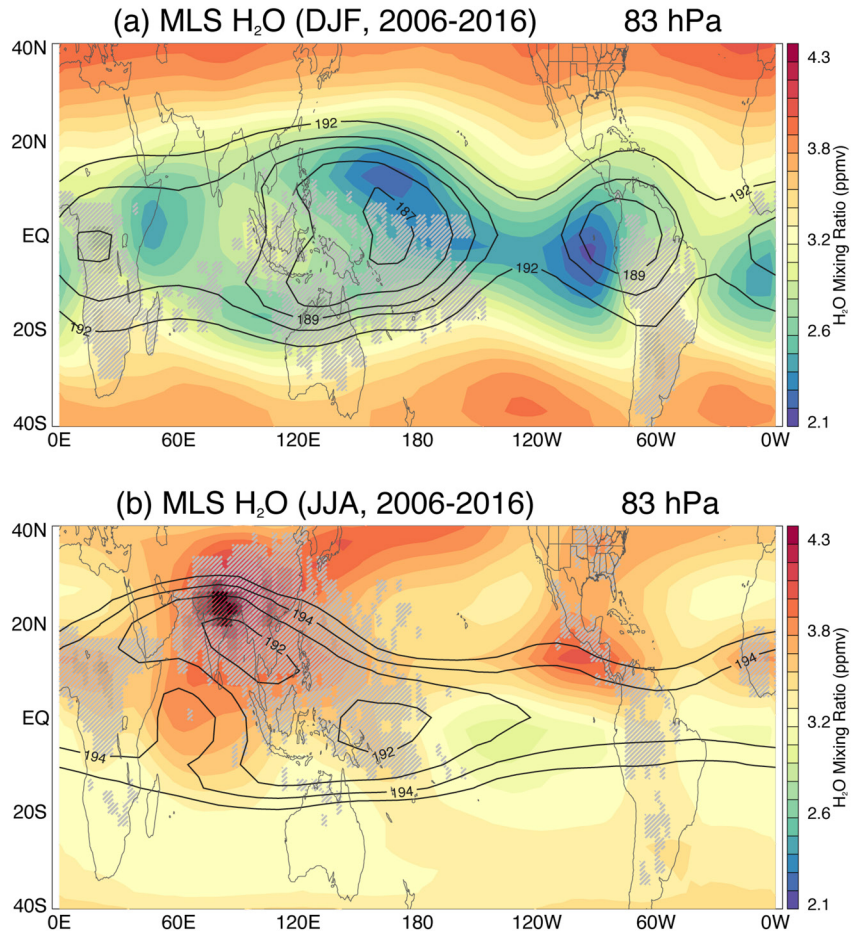


**Figure 1.** Climatological (2006–2016) (a) winter (December–January–February [DJF]) and (b) summer (June–July–August [JJA]) mean water vapor mixing ratios (colored shading) in the lower stratosphere based on Microwave Limb Sounder (MLS) observations at the 83 hPa level. The water vapor field is superimposed with gray shadings representing the occurrence frequency of deep convective cloud tops (>380K) during the respective seasons: light to dark shading represents low to high cloud occurrence frequency. Also shown are contours of the cold-point tropopause temperature climatology from the Global Positioning System radio occultation data for the same time period (see Randel & Wu, 2015).

the tropical stratosphere have been dehydrated by in situ cloud formation, limiting the convective hydration of the tropical uppermost troposphere to at most ~0.5 ppmv (Schoeberl et al., 2018; Ueyama et al., 2015, 2018). These studies also show that the impact of convectively detrained ice crystals on the humidity of the upper troposphere is relatively small compared to the total convective impact (Schoeberl et al., 2014; Ueyama et al., 2020).

We also note that convection can indirectly influence the lower stratospheric water vapor budget by lowering the temperatures in the upper troposphere and lower stratosphere (UTLS). For example, Randel et al. (2015) found that strong convection leads to relatively cooler and thus dry stratosphere (and vice versa) over the summer monsoon regions just above the altitude of maximum convection. This observation is consistent with an earlier model result by Salby and Callagha (2004) that demonstrated a cooling and elevation of the tropical tropopause induced by an intensification or deepening of convection. Our study accounts for the convective modulation of the large-scale temperature field near the tropopause to the extent that this effect is represented in global reanalysis data sets. The detailed relationship between UTLS temperatures and deep convection is currently being investigated in a separate study.

While aforementioned studies suggest that deep convective sources of stratospheric water vapor are generally small (but may be significant on a storm-by-storm case), a quantitative assessment of the convective impact on a global scale such as that of Dauhut and Hohenegger (2022) for the boreal summer requires further investigation. Furthermore, detailed investigation of the year-to-year variability of the convective impact is still lacking. Eulerian

models can represent some important feedback effects, but small-scale processes that impact stratospheric water vapor (including convection, gravity waves, and cloud processes) are often poorly represented unless with high enough resolution (Dauhut & Hohenegger, 2022). Lagrangian models that resolve these small-scale processes are suited to investigate the relative importance of these processes on the stratospheric water vapor budget, although some processes like diffusion are often neglected. Our understanding of the sensitivities of stratospheric water vapor to convective impact is limited in part due to uncertainties in the height of the convective cloud tops as well as its diurnal variability. Therefore, time-resolved, observation-based estimates of convection are critical for an accurate assessment of the convective impact. Since convective activity is likely to change in a warmer climate (e.g., Chou & Chen, 2010; Held & Soden, 2006; Romps, 2011; Tan et al., 2015), there is a need to improve simulations of UTLS processes in global climate models.

In this study, we address the following science questions:

1. What is the impact of convection on the global lower stratospheric water vapor budget?
2. How does the convective impact vary regionally and interannually?
3. What is the dominant mechanism of convective hydration or dehydration?

We first use the backward trajectory (BT) model with a detailed cloud microphysics scheme to investigate the convective impact on global lower stratospheric humidity during boreal winter and summer 2010. We then use the computationally more efficient forward trajectory (FT) model to quantify the interannual variability of the convective impact. The results of this study will provide valuable insights into how future changes in convection may influence the global stratospheric water vapor budget, which then feedback on the climate system and ultimately affect Earth's climate.

## 2. Data and Methodology

### 2.1. Satellite Observation of Lower Stratospheric Water Vapor

One of the main goals of this work is to understand the long-term measurements of lower stratospheric (83 hPa) water vapor from the MLS onboard the Aura satellite. The MLS instrument scans Earth's limb and retrieves approximately 3,500 profiles each day between 82°S and 82°N latitudes. Level 2 version 5 water vapor retrievals (Lambert et al., 2020; Livesey et al., 2020) are analyzed in this study. This version corrects for the temporal calibration drift that appeared around 2010 (Hurst et al., 2016) as well as the dry bias (~20%) below the tropopause; these changes resulted in a 5%–10% reduction in stratospheric water vapor compared to the previous versions (Lambert et al., 2015, 2020; Livesey et al., 2021). The 83-hPa water vapor precision and accuracy are both 7%. The data are screened for quality based on criteria indicated in Livesey et al. (2020).

We focus on boreal winter and summer 2010 for comparison between simulated and observed water vapor fields at the 83 hPa level. Year 2010 was chosen because lower stratospheric water vapor enhancements over the two monsoon regions were particularly clear that summer and resembled those of climatology (Figure 1). Winter 2010 is calculated as the average from December 2009 through February 2010, while summer 2010 is calculated as the average from June through August 2010. We also examine the interannual variations over the 2006–2016 time period. The long-term (2006–2016) seasonal mean water vapor fields shown in Figure 1 are constructed by averaging 7-day averaged data on a 5° latitude × 5° longitude grid over 3 months.

### 2.2. Satellite-Derived Global Convective Cloud Top Altitudes

Current global models have difficulty simulating deep convection and tend to substantially underestimate the occurrence of deep convective clouds penetrating the TTL (e.g., Schoeberl et al., 2018). To accurately quantify the convective impact on the lower stratosphere on a global scale, we require observation-based estimates of the global convective cloud top altitudes at high temporal and spatial resolutions. We use the methodology described in Pfister et al. (2022) with some modifications described below. Based on 3-hourly precipitation measurements from the 3B42 product (i.e., Tropical Rainfall Measuring Mission adjusted merged-infrared precipitation data; Huffman et al., 2007) and the superseding IMERG product (i.e., Integrated Multi-satellite Retrievals for GPM; Huffman et al., 2019), convective regions are first identified by searching for rainfall rates exceeding a threshold value of 0.9 mm $hr^{-1}$ over land and 1.5 mm $hr^{-1}$ over ocean; the different rainfall thresholds account for differences in the structure and microphysics (and thus rainfall rate) of convection over land and ocean. These rainfall thresholds are determined such that the resulting occurrence frequencies of deep convective cloud top heights (e.g., Figure 1) statistically agree with those based on combined CloudSat and Cloud-Aerosol Lidar with Orthogonal

Polarization (CALIOP) observations. A cloud top altitude is estimated by matching the infrared brightness temperature within a given convective region to the local temperature profile from Modern-Era Retrospective Analysis for Research and Applications, Version 2 (MERRA-2; Gelaro et al., 2017) reanalysis. To account for the observed cooling effect of convection near the tropopause (Chae et al., 2011; Selkirk, 1993; Sherwood et al., 2003), the MERRA-2 reanalysis temperatures are modified above the tropopause by calculating a profile that is a mixture of (70%) tropopause air and (30%) environmental air. A 1-km offset is added in the final step since previous studies have shown that infrared methods underestimate the cloud top altitudes by one or more kilometers as compared to lidar measurements (Minnis et al., 2008; Sherwood et al., 2004). This algorithm outputs near global (50°S–50°N) convective cloud top altitudes and potential temperatures every 3 hours at 0.25° latitudes and longitudes. The derived cloud top altitudes agree well with the statistics of the CloudSat and CALIPSO convective cloud tops, and the diurnal cycle is in good agreement with precipitation radar climatology (e.g., Liu & Liu, 2016; Liu & Zipser, 2005). Further details of the convection data set can be found in Pfister et al. (2022).

The climatological mean distribution of deep convection (i.e., cloud tops >380K) shows enhanced activity over distinct regions (Figure 1), most frequently over land. In boreal winter, deep convective clouds are primarily observed over northern Australia, tropical Africa, and South America. They also occur relatively frequently over the tropical western Pacific. In boreal summer, deep convective activity dominates over the Asian monsoon land region as well as over tropical Africa to a lesser extent. Ueyama et al. (2018) used these satellite-derived convective cloud top heights to investigate the impact of convection on the uppermost troposphere during boreal summer. They found that convection was the primary driver of the enhancement in upper tropospheric water vapor over the Asian monsoon region.

Deep convection over the North American monsoon region occurs relatively infrequently based on this data set. As explained by Ueyama et al. (2018), the reasons for this are because (a) the rapid sublimation of ice crystals in the dry stratosphere leaves minimal cloud for detection by infrared satellite measurements, and (b) our mixing assumption above the local tropopause likely underestimates the fraction of stratospheric air in the convective plumes in high shear environments which leads to an underestimation of cloud top potential temperatures (Homeyer et al., 2017). For the purpose of a case study to quantify the sensitivity of lower stratospheric water vapor to convective cloud top heights, we correct for the underestimated cloud tops over North America by modifying the convective cloud top potential temperatures over the northern midlatitudes in year 2010 when lower stratospheric water vapor was particularly enhanced over the North American monsoon region. Instead of assuming that convection overshooting the tropopause mixes with 70% tropospheric and 30% stratospheric air, we use a 50-50 mixture in northern midlatitudes. This modification corresponds to a warmer plume due to more entrainment, and thus the inferred cloud tops are higher in altitude and potential temperature. The resulting global distribution of deep convective clouds in 2010 resembles the climatological mean distribution shown in Figure 1, except for a fivefold increase in the maximum occurrence of deep convective cloud tops (above 380K potential temperature level) over the continental United States during summer (not shown). The temperature profiles above the tropopause based on 70%/30% and 50%/50% mixing assumptions are both well within the estimated range of the cooling effect of overshooting convection from previous works (Adler & Mack, 1986; Griffin et al., 2016).

To permit comparisons with previous studies utilizing this cloud top data set (e.g., Schoeberl et al., 2018; Ueyama et al., 2015), we have used the original (unmodified) version for model comparison and for the investigation of the interannual variability of the convective impact. Figure 2a shows the interannual variability of global deep convective activity in boreal winters and summers from 2006 through 2016. Various modes of climate variability, such as the El Niño-Southern Oscillation (ENSO), presumably affect the global convective activity. Deep convection was relatively active in year 2010, which began with an El Niño winter followed by a weak La Niña summer. The simulated lower stratospheric water vapor fields during boreal winter and summer 2010 are evaluated in Section 3.1. It is evident from Figure 2b that deep convective activity is particularly large over the Asian monsoon region in boreal summer, although convective activity over the North American monsoon region exhibits similar year-to-year variability with smaller magnitude. We will explore the relationship between year-to-year variations in deep convection and estimated convective impact on the UTLS using the FT model in Section 3.2.

### 2.3. Model Description

#### 2.3.1. BT Model Approach

The BT model approach generally follows the methodology of Ueyama et al. (2015, 2018, 2020) and is summarized in Table 1. We first calculate 75-day BTs from 2° latitude × 2° longitude grid points in a given domain at the

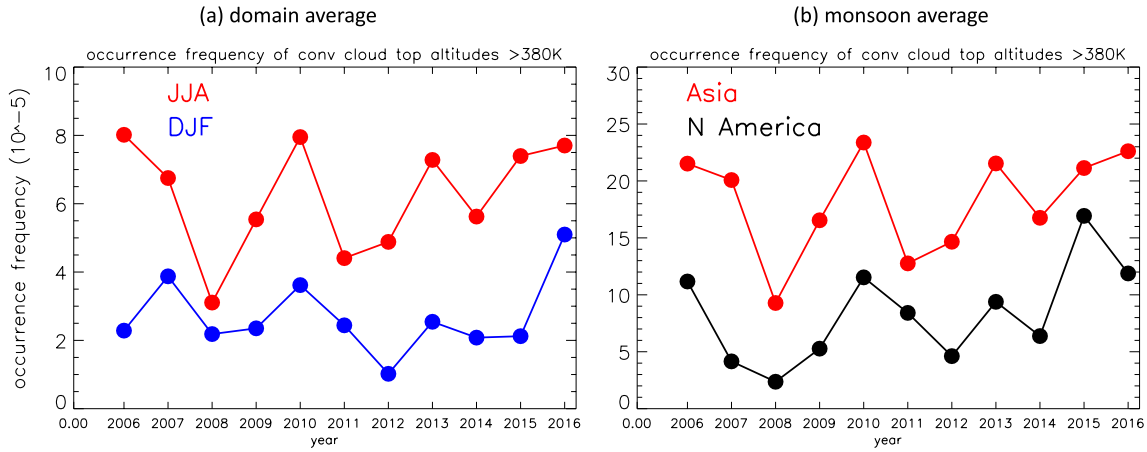


**Figure 2.** (a) Time series of the occurrence frequency of deep convection (cloud tops above the 380K potential temperature level) over 30°S–30°N in winter and 20°S–50°N in summer during 2006–2016. (b) As in (a) but for the Asian (red; 0°–45°N, 0°–180°E) and North American (black; 0°–45°N, 0°–180°W) monsoon regions during summer. Occurrence frequencies over the North American monsoon region are multiplied by a factor of 10. Occurrence frequency from December 2005 through February 2006 is plotted as the winter 2006 value.

390K potential temperature level corresponding to a level in the lower stratosphere just above the climatological domain-averaged tropopause. For the winter simulation, we initialize the BTs from 30°S to 30°N domain on 21 February 2010 going back in time to early December 2009. For the summer simulation, we initialize the BTs from 20°S to 50°N domain on 22 August 2010 going back to early June 2010. Trajectories are calculated using hourly horizontal wind data from the fifth generation of European Center for Medium-range Weather Forecast reanalysis (ERA5; Hersbach et al., 2020). ERA5 data used in this study are available at every 0.3° latitude-by-longitude grid at 29 levels between 50 and 300 hPa levels with ∼5 hPa resolution in the UTLS (e.g., 73, 78, 83, 89, 94, 101, and 107 hPa). For the vertical motions of the parcels, we use a combined broadband flux and heating rate product of the CloudSat, Cloud-Aerosol Lidar and Infrared Pathfinder Satellite Observations (CALIPSO) and Moderate Resolution Imaging Spectroradiometer (MODIS) missions (2B-FLXHR-LIDAR version R05; Henderson et al., 2013; L'Ecuyer et al., 2008). Due to the lack of global coverage of the satellite-based heating rates at high enough resolution, the data are averaged over a 3-month period to compute seasonal means (December–January–February for winter, June–July–August for summer). Although there is large uncertainty associated with an individual trajectory pathway, the averaging over thousands of trajectories within a large domain captures the transport characteristics of air masses through the UTLS reasonably well (Bergman et al., 2012).

After the trajectories have been calculated, we extract vertical profiles (from the 350–430K potential temperature levels) of ERA5 temperatures at each time step along each trajectory path to generate time versus height "curtains" of temperatures. Although the effect of high-frequency gravity waves on TTL humidity appears to be small (Fueglistaler & Baker, 2006; Schoeberl et al., 2014, 2015; Ueyama et al., 2015), gravity waves have been shown to affect cloud microphysical properties (Dinh et al., 2016; Jensen & Pfister, 2004) and increase the occurrence of in situ formed clouds due to their modulation of the cooling rates (Schoeberl et al., 2015, 2016; Ueyama et al., 2015). We therefore add the effects of these waves on the temperature curtains using the gravity wave spectra calculated from Project Loon's lower stratospheric superpressure balloon measurements (Schoeberl et al., 2017) similar to the climatological mean high-frequency gravity wave spectra described in Jensen and Pfister (2004).

The temperature curtains, along with curtains of heating rates, are used to drive the one-dimensional (column) cloud microphysical model in the next step. Specifically, the cloud model is initialized with the 7-day mean gridded MLS water vapor profile nearest to the parcel location at the earliest time of the trajectory (i.e., 75 days before the BT launch date). Cloud ice processes such as nucleation, deposition growth, sedimentation, and sublimation are then simulated in one-dimensional (vertical) space along each trajectory path (from the earliest to latest time in the forward direction). For example, homogeneous ice nucleation is triggered when the ice saturation mixing ratio exceeds a threshold of ∼1.6 (Koop et al., 2000). We do not include heterogeneous ice nucleation processes (which are triggered at a lower supersaturation of ∼1.3) since Ueyama et al. (2015) have shown that water vapor and clouds in the TTL are relatively insensitive to the heterogeneous freezing process. The heating rate curtains also enable the proper treatment of ice sedimentation and water vapor vertical redistribution.

**Table 1**
*Model Configuration and Characteristics of the Backward and Forward Trajectory Modeling Approaches Used in This Study*

| | Backward trajectory model | Forward trajectory model |
|---|---|---|
| Parcel launch method | • 2° lat × 2° lon grid within a domain (30°S–30°N for winter, 20°S–50°N for summer)<br>• At 390K potential temperature level<br>• At a given date (21 February 2010 for winter, 22 August 2010 for summer) | • At the tops of convective clouds within the 40°S–40°N domain<br>• Continuously every 6 hr starting in year 2000 |
| Trajectory length | 75 days | Variable |
| Reanalysis (T, U, V) data | Hourly ERA5 data at 0.3° lat × 0.3° lon resolution at 29 levels between 50 and 300 hPa | 6-hourly MERRA-2 data at 0.5° lat × 0.635° lon resolution (interpolated to 2° lat × 2° lon grid) at 45 levels between 5 and 50 km |
| Diabatic heating rates | Satellite-based heating rates[a] available at 2.5° lat × 2.5° lon × 239 m resolution averaged over 3 months (DJF, JJA) | MERRA-2 (same resolution as T, U, V data) |
| Convection scheme | Satellite-based convective cloud top heights[b] available every 3 hr at 0.25° lat × 0.25° lon resolution | Satellite-based convective cloud top heights[2] available every 3 hr at 0.25° lat × 0.25° lon resolution |
| Gravity wave scheme | Gravity wave spectra from lower stratospheric superpressure balloon measurements[c] | Gravity wave spectra from lower stratospheric superpressure balloon measurements[3] |
| Cloud scheme | One-dimensional column model where cloud microphysical processes such as nucleation, deposition growth, sedimentation, and sublimation are simulated in vertical space along each trajectory path. | Zero-dimensional cloud model that tracks the mean ice crystal number density, mass, and size, as well as the water vapor mixing ratio. Sedimentation, deposition growth, and sublimation are approximated. |
| Advantages | • Provides direct estimates of water vapor at the desired locations<br>• Provides information about source and history of air parcels<br>• Detailed cloud microphysical model accounts for vertical redistribution of water by ice cloud processes. | • Computational efficiency allows for good statistics from abundant parcel tracking.<br>• Provides continuous picture of the time evolution |
| Limitations | • Does not correctly represent air parcel age distribution if the mean age exceeds the trajectory integration time<br>• Lack of mixing between parcels<br>• Assumes no vertical wind shear of the horizontal wind along the trajectories[d]<br>• Trajectories need to be sufficiently long for the parcels to traverse through the cold tropopause temperatures. | • Does not provide detailed information about air parcel origins and pathways<br>• Results influenced by parcel launch locations<br>• Lack of mixing between parcels<br>• Ice sedimentation loss rate calculation requires an assumption of the parcel (cloud) depth<br>• Cloud parameterization assumes monodispersed ice crystal size distribution. |

*Note.* See also descriptions in the following references for the backward (Jensen & Pfister, 2004; Ueyama et al., 2015, 2018, 2020) and forward (Schoeberl & Dessler, 2011; Schoeberl et al., 2014, 2016) trajectory model approaches.

[a]2B-FLXHR-LIDAR (L'Ecuyer et al., 2008; Henderson et al., 2013). [b]See Section 2.2 and Pfister et al. (2022). [c]See Schoeberl et al. (2017). [d]Applies to the curtain model approach used in this study.

Ice crystals formed after nucleation are assumed to be in thermal equilibrium with the ambient air. Thus, if an ice crystal encounters subsaturated or supersaturated air, it will sublimate or grow by deposition, respectively. To model the cloud evolution, the sizes and heights of thousands of individual ice crystals are tracked throughout their lifetime; no assumptions are made about these ice crystal properties, which are calculated dynamically by the model. Water vapor is treated in an Eulerian one-dimensional grid, and the water exchange between the vapor and condensed phases is computed at each time step. The vertical advection of water vapor and ice crystals (including sedimentation of ice) is diagnosed using the heating rate curtains. In this way, this column cloud microphysical model properly treats the vertical redistribution of water by clouds.

The water and cloud evolution along the trajectory path can be affected by an encounter with a convective cloud. To diagnose the convective influence, we trace the BTs through time-varying global convective cloud top altitude fields (described in Section 2.2) to identify convective cloud encounters along each trajectory path. Whenever a trajectory intersects a convective cloud, the column model is saturated up to the cloud top potential temperature. Convection will hydrate the environment if the air is initially subsaturated, while it will dehydrate the environment if the air is initially supersaturated. In situ measurements near convection indicate frequent supersaturation in the tropical upper troposphere (e.g., Krämer et al., 2020), while overshooting convection into the lower stratosphere will most likely encounter dry, subsaturated air. Deep convection often deposits ice crystals near the cloud

top to form anvil cirrus, but convectively detrained ice crystals in aging anvils have a relatively minor impact on TTL humidity (Ueyama et al., 2020). To quantify their impact on lower stratospheric humidity, monodispersed ice crystals of diameter 30 μm with an ice water content of 30 ppmv are added in the column model up to the cloud top potential temperature, consistent with aircraft observations (Frey et al., 2011, 2014, 2015; Jensen et al., 2009; Krämer et al., 2020). When comparing the simulated water vapor ratios to those of MLS observations, we apply the MLS averaging kernel on the simulated water vapor profiles on the final day (i.e., BT launch date) and compare the values at the 83 hPa level.

The BT method provides direct estimates of the water vapor at the desired locations, which in this case is the global lower stratosphere. The limitations of any BT method include the need to run separate sets of trajectories for each valid time and the lack of mixing between parcels. Inter-parcel mixing along the trajectories (which is ignored here) has been found to potentially increase the humidity of the lower stratosphere particularly around the subtropical jets in the summer hemispheres (Poshyvailo et al., 2018) and near hydration patches (Dauhut & Hohenegger, 2022; Lee et al., 2019). The simulated water vapor mixing ratios are averaged over the 5° latitude × 5° longitude grid to crudely represent the mixing of air parcels. Furthermore, the BT "curtain" approach assumes no vertical wind shear of the horizontal wind along the trajectories. The laminar structure of TTL cirrus clouds clearly suggests the presence of vertical wind shear in the UTLS region. However, given the relatively short lifetimes of wide-scale cirrus clouds on the order of 1–2 days (Jensen et al., 2011), the dehydration and rehydration effects of cloud processes on the water vapor profile appear to be relatively insensitive to vertical wind shear. Furthermore, simulating water vapor profiles based on trajectories launched at other potential temperatures, thereby accounting for the different trajectory paths above and below the 390K level, has little impact on the overall conclusions of this study. Another drawback is that when ascent rates in the UTLS are relatively slow such as during summer, BTs need to be sufficiently long for the parcels to traverse through the cold temperatures near the tropopause. If a parcel does not descend far enough below the tropopause (in reverse time), clouds will not form along the trajectory (in forward time), and the initialized MLS water vapor mixing ratio propagates forward *unless* the parcel intersects with convection. Although only ∼10% of the summertime parcels at the 390K potential temperature level descend below the 370K level in 75 days, nearly all (>99%) of the parcels encounter convection and/or form clouds along the 75-day trajectories, allowing a quantitative assessment of the global mean impact of convection.

#### 2.3.2. FT Model Approach

The FT model approach follows the forward domain filling methodology of Schoeberl and Dessler (2011) and is compared to the BT model approach in Table 1. In previous studies, parcels in the FT model were released on a fixed latitude-by-longitude grid at a specified potential temperature surface (typically between 360 and 370K) just above the level of zero tropical radiative heating; this ensures that the parcels ascend into the stratosphere rather than immediately descend back into the lower troposphere. In this study, about 40,000 parcels are continuously released every 6 hr at each convective cloud top above 330K (∼10 km) over the 40°S to 40°N latitude domain. This method is more consistent with the BT approach described in Section 2.3.1, where parcels in the lower stratosphere are tracked backward in time and intercept convective clouds along their trajectories. The FT parcels are initialized with the climatological (2005–2015) daily mean MLS water vapor mixing ratio at that location, though the results are not sensitive to the initial water vapor value. At the end of each day, any parcels that have descended below the 340K level are removed, as well as those parcels that have reached the model top at ∼2,500K level (about 0.4 hPa or 55 km). The model reaches a quasi-steady state with ∼500,000 parcels after several years of integration.

The FTs are calculated based on the Bowman trajectory model (Bowman, 1993; Bowman & Carrie, 2002) using 6-hourly horizontal winds and diabatic heating rates from MERRA-2. MERRA-2 data at 0.625° longitude × 0.5° latitude resolution is interpolated to 2° longitude × 2° latitude grid at each of the 45 layers between 5 and 50 km; the reduction in spatial resolution has minimal impact on our results since smaller scale waves are included in the gravity wave parameterization. The impact of other small-scale processes, such as eddies and turbulence, is assumed to be small. We use a simplified zero-dimensional cloud model that tracks the mean ice crystal number density, mass, and size, as well as the water vapor mixing ratio (Fueglistaler & Baker, 2006; Schoeberl et al., 2014, 2016). Ice nucleation is triggered when the ice saturation ratio exceeds a threshold of 1.6, as in the BT approach. The number of ice crystals depends on the cooling rate derived from Kärcher et al. (2006), which is modulated by the same high-frequency gravity wave spectra as in the BT approach. The total ice mass

is computed from the ice volume mixing ratio and density of ice at the parcel temperature. Ice particle effective radius is then calculated by dividing the total ice mass by the number of particles, all of which are assumed to be spherical. The simplified cloud model calculates ice crystal growth by deposition based on temperature, saturation, and particle radius. It also simulates ice crystal loss by sedimentation where the sedimentation loss rate is inversely proportional to the assumed parcel vertical dimension of 500 m based loosely on CALIOP observations. Important differences between the BT and FT model approaches are that the microphysical scheme of the BT model allows for the tracking of numerous individual ice crystals and the sublimation of falling hydrometeors (Table 1).

Similar to the convective influence analysis of the BT parcels, convective encounters of FT parcels are identified by tracking the parcels through the time-varying, satellite-derived convective cloud top altitude field. At each convective encounter, the parcel is saturated (i.e., relative humidity is reset to 100%) and a small amount of ice is added. The number and size of convective ice crystals added are based on tropical convection observations of Frey et al. (2014; see their tab. 1). The water vapor mixing ratios of parcels scattered over the lower stratospheric domain during the winter and summer months are averaged into fixed latitude-by-longitude grid and compared with seasonal mean MLS water vapor at the 83 hPa level. This averaging crudely simulates parcel mixing, as mentioned above. Since the water vapor mixing ratios at the 83 hPa level in the FT model are not greatly affected by the MLS averaging kernel due to the linear water vapor gradient above ∼150 hPa (not shown), the averaging kernel was not applied to the FT model results for faster computation.

The FT model approach has the advantage of providing a time series of the full three-dimensional water vapor field throughout the stratosphere from a single simulation. However, the FT model does not save the individual parcel paths like the BT model. Instead, the location and time of specific events (e.g., last dehydration event or tropopause crossing) are recorded. The two models are also configured to use different reanalysis fields (Table 1). The implications of these model differences are discussed in the next section.

## 3. Results

### 3.1. Winter and Summer 2010

#### 3.1.1. Model Evaluation

The 83-hPa water vapor fields in boreal winter and summer 2010 are simulated in the BT and FT models and evaluated against their corresponding MLS observations in Figures 3 and 4. The BT simulation is for a single day (due to computational limitations), whereas the MLS and FT model fields are for a 7-day period.

The 7-day mean water vapor field centered on 21 February 2010 (i.e., 18–24 February 2010) exhibits significant spatial variability with regional-scale anomalies (Figure 3a). The BT model does not place the water vapor anomalies in the exact location as observed by MLS partly because the simulated water vapor field is for a single day (Figure 3c). The magnitude and location of the water vapor anomalies vary significantly on a weekly basis as well as from year to year (not shown). Also, even though the MLS averaging kernel is applied to the simulated water vapor profiles, the simulated profiles are based on BTs calculated from a single level (390K) and thus may not capture relatively shallow water vapor features found in the observations above and below the BT launch level. Nonetheless, the large-scale pattern resembles that of observations with the driest regions over the deep tropics. The observed dryness of the southern tropics and the maritime continent is underestimated in the BT model, yielding an overall moist bias (+0.14 ppmv) of the BT model in boreal winter (Figure 3e). In contrast, the FT model exhibits an overall dry bias (−0.03 ppmv), especially in the southern hemisphere over Africa and South America (Figures 3d and 3f), which is likely associated with assumptions made in the simple cloud microphysics scheme as described in Section 3.1.2. Despite these model differences, both models simulate minimum water vapor over equatorial South America, which coincides with the region of minimum cold-point tropopause temperature (Figure 3b). Differences in the lower stratospheric water vapor distribution in winter 2010 compared to that of climatology (Figure 1a) are partly associated with ENSO variability, as mentioned earlier.

The lower stratospheric water vapor field during boreal summer 2010 (Figure 4a) consists of large enhancements over the Asian and North American monsoon regions, as seen in climatology (Figure 1). The 7-day mean water vapor field centered on 22 August 2010 (i.e., 19–25 August 2010) indicates a relatively moist stratosphere over the western and central Pacific, which may be associated with the transient eastward transport of moist air from

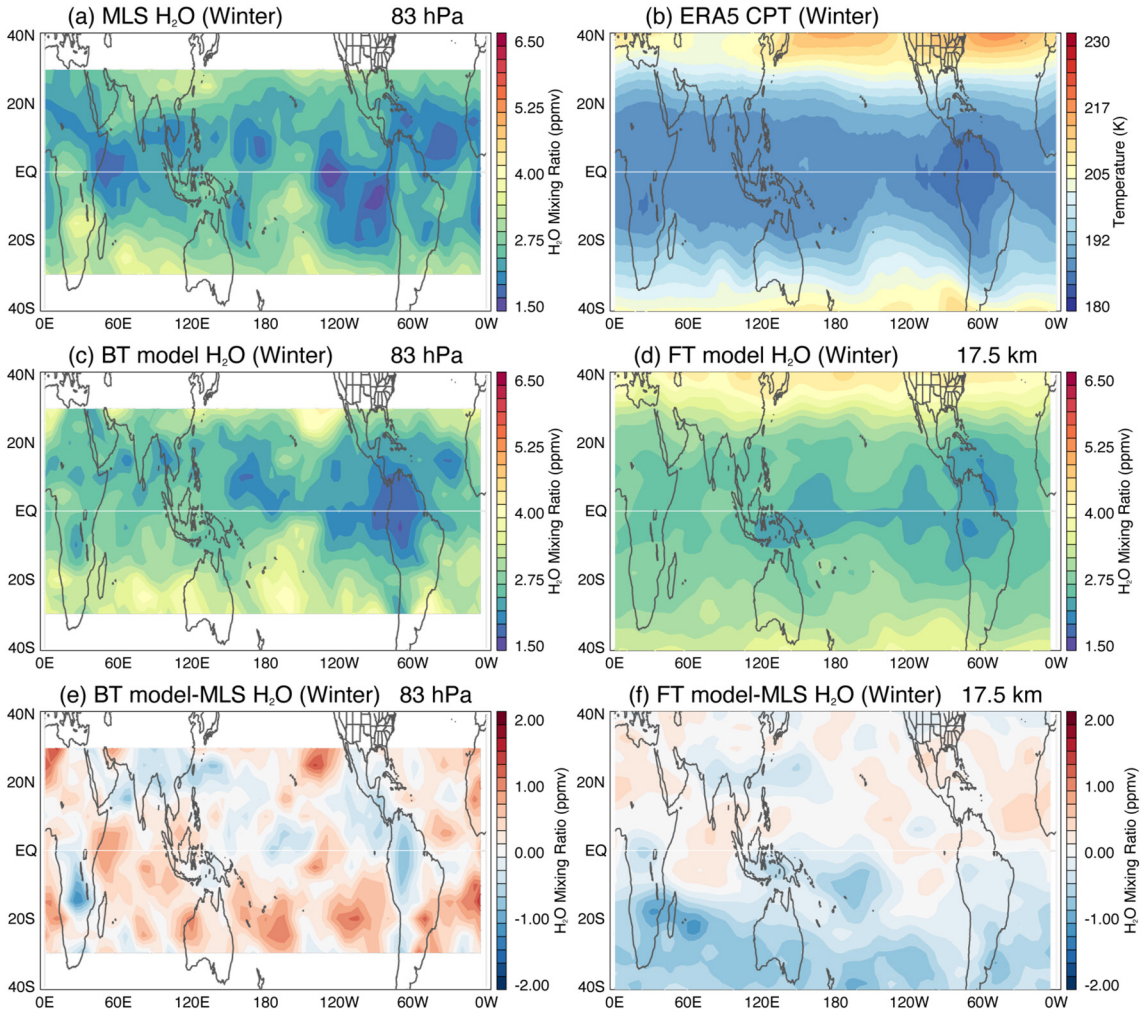


**Figure 3.** Lower stratospheric (83 hPa) water vapor field in boreal winter (21 February 2010) as observed by Microwave Limb Sounder (MLS) (a) and simulated in the backward and forward trajectory models ((c) and (d), respectively). (e) and (f) Water vapor difference (model minus MLS) fields. (b) Cold-point tropopause temperature field from ERA5 during the same time period. MLS, fifth generation of European Centre for Medium-range Weather Forecast reanalysis (ERA5), and forward trajectory (FT) model data are averaged over 7 days centered on 21 February 2010. Note that (f) is calculated with respect to the 7-day mean MLS field gridded onto the FT model grid, which is similar but not identical to (a). 1-2-1 smoothing is applied to all the data for presentation purposes.

the Asian monsoon region. The 83-hPa water vapor field simulated in the BT model (Figure 4c) is dominated by the elevated water vapor mixing ratios over the Asian monsoon, in agreement with observations, although there are some differences in the placement of these anomalies due to the simulation being for a single day. The water vapor enhancement over the North American monsoon region is not as large or spatially coherent as in observations. However, it is an improvement over the previous simulation using the same model (see Figure 3 in Ueyama et al., 2018) with ~0.2 ppmv increase in the regional mean water vapor mixing ratio. The main difference between the two versions is the modification of the convective cloud top heights over the northern midlatitudes that assumes more mixing between tropospheric and stratospheric air, as described in Section 2.2.

Lower stratospheric water vapor over the two summer monsoon regions is also enhanced in the FT model (Figure 4d), but the model is generally too dry compared to MLS observations (Figure 4f). One possible explanation is that the FT model is underestimating the spread of cirrus anvils that would widen the convective moistening impact. A second explanation is that the height of the convection is underestimated over certain regions. The sensitivity of global lower stratospheric water vapor to convective cloud tops of varying heights over various regions in the two models will be investigated in a future study. In the current setting, biases are no more than ~10% of the observed domain-averaged water vapor mixing ratios in the BT model for both winter and summer 2010.

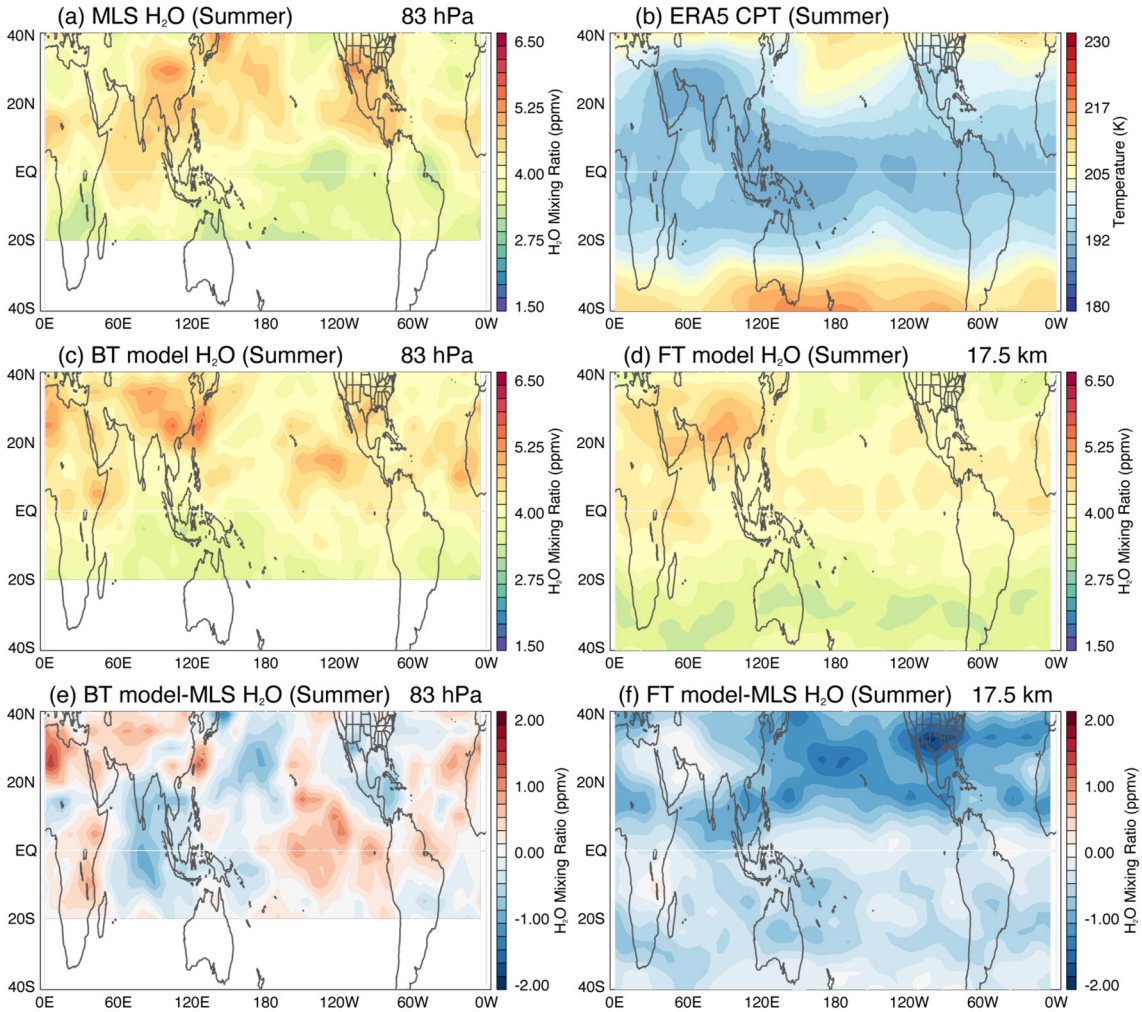


**Figure 4.** Lower stratospheric (83 hPa) water vapor field in boreal summer (22 August 2010) as observed by Microwave Limb Sounder (MLS) (a) and simulated in the backward and forward trajectory models ((c) and (d), respectively). (e) and (f) Water vapor difference (model minus MLS) fields. (b) Cold-point tropopause temperature field from the fifth generation of European Centre for Medium-range Weather Forecast reanalysis (ERA5) during the same time period. MLS, ERA5, and forward trajectory (FT) model data are averaged over 7 days centered on 22 August 2010. Note that (f) is calculated with respect to the 7-day mean MLS field gridded onto the FT model grid, which is similar but not identical to (a). 1-2-1 smoothing is applied to all the data for presentation purposes.

Another method for evaluating the models is to compare the simulated cloud fractions to those observed by CALIOP. The BT model simulates the cirrus cloud distributions in the UTLS remarkably well during both seasons with correlation coefficients greater than 0.9, although the model slightly overestimates the amount of clouds in both seasons (not shown). The FT model also simulates the cirrus cloud distributions reasonably well, but underestimates the cloud fractions by 30% in winter and 48% in summer 2010 compared to CALIOP measurements. The simplified cloud scheme that is coupled to the FT model removes settling particles once they reach the lower edge of the cloud domain, which would tend to underestimate the cloud occurrence. However, interannual variations in lower stratospheric water vapor are simulated reasonably well in the FT model, as will be shown in Section 3.2 and demonstrated in Dessler et al. (2014). Thus, we will primarily use the FT model to examine the amplitude of the year-to-year variations in the convective impact relative to its mean.

### 3.1.2. Convective Impact

To investigate the impact of convection on lower stratospheric humidity, we have also run a set of simulations without the convective effects. In the "no convection" simulations, trajectory intersections with convection are simply ignored (i.e., no changes are made to the water vapor or ice at that time). The convective impact on lower stratospheric water vapor is then quantified by subtracting the 83-hPa water vapor mixing ratios simulated

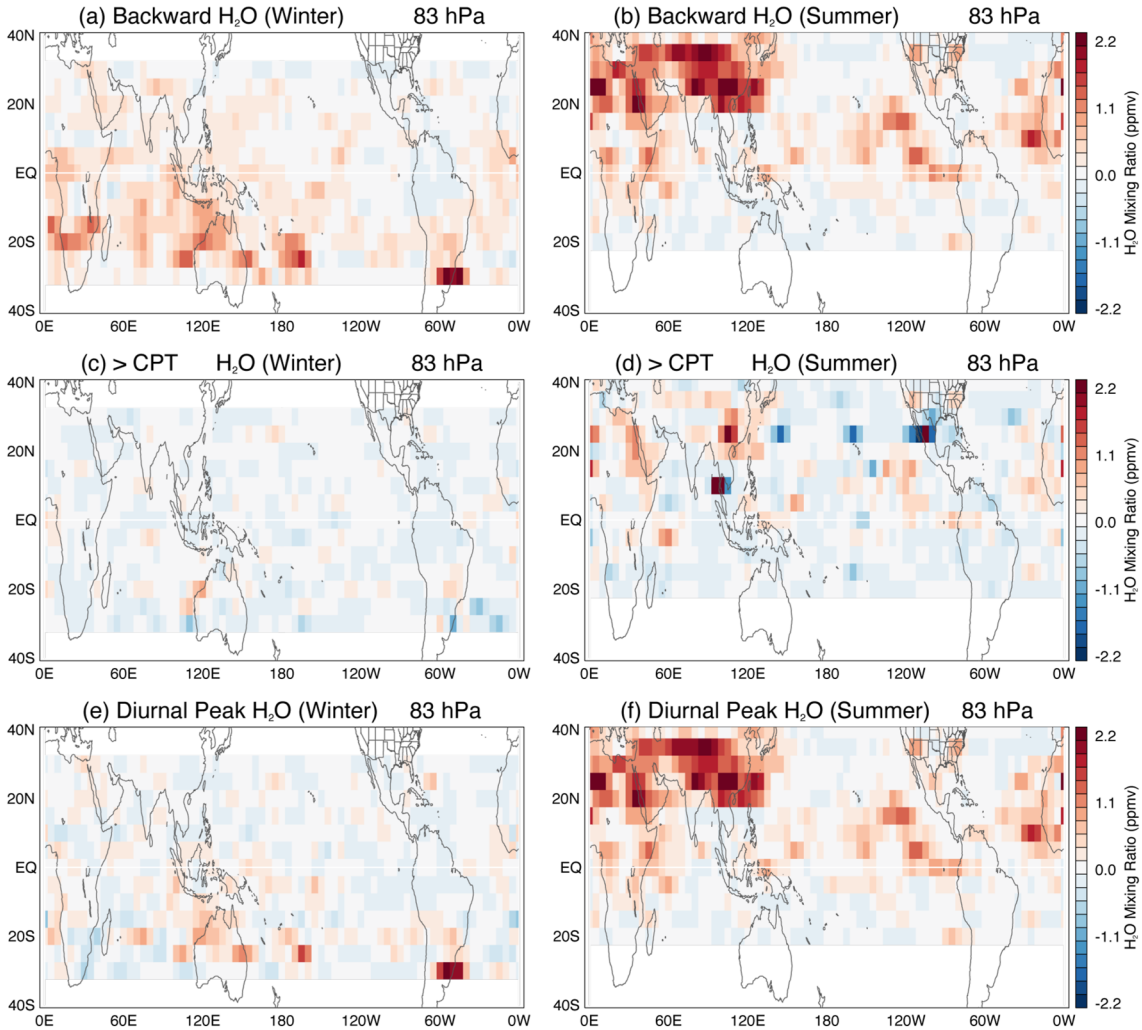


**Figure 5.** Impact of convection on the lower stratospheric (83 hPa) water vapor field during (left) winter and (right) summer 2010 based on the backward trajectory model approach: impact of (a, b) all convective clouds above 350K, (c, d) convective cloud tops above the local cold-point tropopause, and (e, f) diurnal peak in convective cloud top height.

without convection from those simulated with convection of their respective models. The model biases described earlier may impact the estimates of the convective impact. However, given that the model biases are no more than 10% of the observations, the assumption here is that the estimated convective impact is relatively insensitive to the model biases.

The convective impact on lower stratospheric water vapor during winter and summer 2010 estimated from the BT model is shown in Figure 5. It is evident that the overall effect of convection is a moistening of the lower stratosphere (Figures 5a and 5b). In winter, convective hydration occurs mostly south of the equator with largest moistening over northern Australia, where the relatively frequent deep convection occurs. Convective impact is minimal over the cold temperature region of the western tropical Pacific because convectively injected water vapor and ice are quickly removed by the freeze-drying process. In summer, convection increases the humidity over the Asian monsoon region by ~1 ppmv (regional mean increase of 30%), dominating the global convective impact. Maximum enhancement in water vapor in boreal summer coincides with the region of frequent deep convective occurrence located to the north of the coldest temperature region (Figure 1b). Furthermore, while convection has little impact on the freeze-drying location over the tropical Pacific in boreal winter, summertime convection tends to shift the freeze-drying location to the northwest of the cold temperature region, as in previous studies (see fig. 8 in Ueyama et al., 2015, and figs. 9 and 10 in Ueyama et al., 2018). Thus, the degree of convective moistening at a given location and time is likely to be modulated by local temperatures (i.e., saturation

level), consistent with the overall understanding that lower stratospheric humidity is strongly controlled by transport through the cold tropopause (Brewer, 1949; Holton & Gettelman, 2001; Randel & Park, 2019). Convective moistening over the North American monsoon region is not as large (0.2 ppmv corresponding to a regional mean increase of 5%) as that over the Asian monsoon and instead centered over the eastern tropical Pacific. Northern Africa is also moistened by convection, contributing to the BT model moist bias compared to MLS observations (Figure 4e). These large-scale features of the convective impact are observed in simulations of lower stratospheric water vapor on other days within the same 1-week time period in each season.

The domain-averaged moistening is about 0.3 ppmv or 10% in both seasons (0.28 ppmv in winter and 0.32 ppmv in summer), in agreement with Schoeberl et al. (2014) and Dauhut and Hohenegger (2022). Sensitivity simulations with the BT model indicate that convection moistens the lower stratosphere by increasing the relative humidity of the subsaturated environment; the impact of convectively detrained ice crystals in aging anvils is small, in agreement with Ueyama et al. (2020) for the winter TTL. The convective impact is larger (i.e., approximately 0.4 ppmv in winter and 0.6 ppmv in summer) and more spatially uniform in the FT model (not shown). It is reasonable to expect some differences in the results based on the BT and FT models due to differences in the modeling approaches (Table 1). First, the two models use different reanalysis fields to calculate the trajectories and to simulate the cloud processes. Ideally, the two models will use the same reanalysis data, but the models are each set up to run with specific reanalysis products. The BT model is configured to use high-resolution ERA5 data over a short time period, while the FT model is configured to use low-resolution MERRA-2 data over multiple years. Tegtmeier et al. (2020) investigated the differences in the TTL temperature and tropopause characteristics from various reanalyses data and found that TTL temperatures from ERA5 are colder (by ∼0.5K) than those of MERRA-2 in the climatological mean as well as in year 2010. This suggests that differences in the temperature data alone would yield a drier lower stratosphere in the BT model using ERA5 temperatures than in the FT model using MERRA-2 temperatures, opposite of our findings. Second, a few of the BTs terminate in stratospheric locations, and thus will be wetter than the FTs that move through the tropopause. Third, as noted earlier, the microphysical scheme of the BT model allows for the sublimation of falling hydrometeors. The overall moistening of the UTLS by this effect in the BT model likely counteracts the differences due to the reanalysis temperatures. Fourth, the different heating rates could impact the model results. Sensitivity simulations using seasonal mean and hourly ERA5 heating rates in the BT model suggest that the convective impact on lower stratospheric water vapor varies by only a few percent in winter and summer 2010. This is likely because cloud impacts on TTL humidity build-up over periods of weeks, which is much faster than the vertical transport time scale through the TTL on the order of 1–2 months. Overall, the differences in the two models provide us with some assessment of the uncertainty in the calculation.

To evaluate the importance of extreme deep convection overshooting the local tropopause on global lower stratospheric water vapor budget, we run the BT model with convective cloud tops capped at the cold-point tropopause altitudes derived from ERA5 reanalysis data. We find that convection overshooting the cold-point tropopause increases global lower stratospheric humidity by only 1% in boreal winter and summer 2010 (Figures 5c and 5d), which is an order of magnitude smaller than the total convective impact of 10%. Regionally, tropopause-overshooting convection moistens the lower stratosphere over the Asian monsoon region by ∼6% during summer. The largest impact during winter is observed over northern Australia and southeastern coast of South America, which correspond to the regions of frequent extreme deep convection. It is worth noting that while the effect of tropopause-overshooting convection may be small, the bulk of the direct convective moistening of the lower stratosphere during boreal summer is due to deep convection reaching >370K potential temperature level primarily found over the Asian summer monsoon region (Figure 1b). The small impact of tropopause-overshooting convection on lower stratospheric water vapor is consistent with the infrequent occurrence of these events (approximately 5% and 8% of all convective clouds in winter and summer, respectively) and the findings of Jensen et al. (2020). However, an important caveat is that these results are based on satellite-derived convective cloud top altitude estimates with uncertainty of ∼0.5–1 km (Pfister et al., 2022). If the vertical extent and/or frequency of deep convective events are underestimated over some regions, and if we account for the potential mixing above the cloud tops (Dauhut et al., 2018; Lane, 2008), the impact of tropopause-overshooting convection on lower stratospheric water vapor may indeed be much higher than that found in this study. In general, the globally averaged lower stratospheric water vapor exhibits weak sensitivity to small changes in the height of the global convective cloud tops (i.e., an increase in global lower stratospheric water vapor of 0.01 ppmv for a kilometer increase in global convective cloud tops).

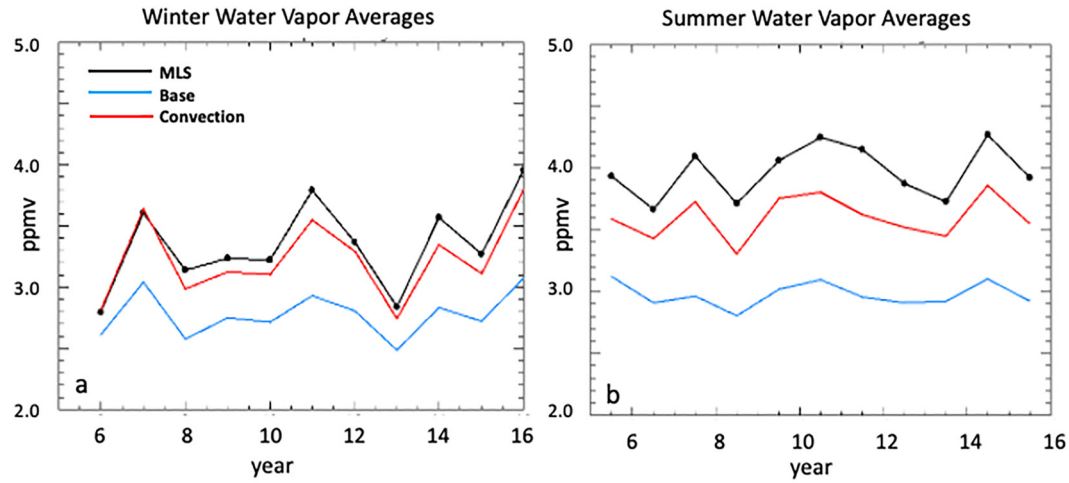


**Figure 6.** Time series of the domain averaged (30°S–30°N for winter, 20°S–50°N for summer) lower stratospheric water vapor mixing ratio during (a) winter and (b) summer 2006–2016: Microwave Limb Sounder (MLS) observations (black), model without convection (blue), and model with convection (red). Winter is the average of December through February of the year of January, and June through August is represented as the summer value.

Convection exhibits a distinct diurnal cycle with a large peak around 1630 local time over land and a smaller peak at around 0430 local time over the ocean (Liu & Liu, 2016; Liu & Zipser, 2005). We examine the impact of the diurnal peak in convective cloud top altitudes by first constructing time-varying global convective cloud top altitude data without the diurnal peak in convection: the 3-hourly convective cloud top altitudes (00, 03, 06, 09, 12, 15, 18, and 21Z) on a given day are replaced with the cloud top altitude at 00Z of that same day. We then trace the backward trajectories through this modified convection data set to examine the sensitivity of lower stratospheric humidity to the diurnal peak in convective cloud top altitudes. Note that the cloud top altitude at 00Z is roughly equivalent to the daily mean cloud top altitude over land, while it is slightly lower than the diurnal peak in cloud top altitude over the ocean. We find that the diurnal peak in convection moistens the lower stratosphere by approximately 0.1 ppmv in winter and 0.3 ppmv in summer (Figures 5e and 5f). In other words, the diurnal peak in convection is responsible for about half of the total convective moistening of the lower stratosphere during winter and nearly all of the convective moistening during summer. The impact of the diurnal variability of convective cloud tops over various regions will be explored in detail in a future study.

### 3.2. Interannual Variability

In this section, we use the FT model to examine the year-to-year variability in lower stratospheric water vapor as well as the variations in the convective impact. The time series of domain-averaged water vapor mixing ratios at the 83 hPa level in winter and summer of each year from 2006 to 2016 are shown in Figure 6. The model captures the year-to-year variability in lower stratospheric water vapor remarkably well, as seen by the good agreement with MLS observations. During this time period, the global lower stratospheric water vapor varied between ~2.8 and ~4 ppmv in winter and between ~3.5 and ~4.3 ppmv in summer. Winter 2010 appeared to have been an average year, whereas summer 2010 appeared to have been a relatively moist year during this time period.

Also shown are domain-averaged water vapor mixing ratios in the simulation without convection (blue lines). As expected, the lower stratosphere in the simulation without convection is much drier than in the simulation with convection. However, even without the impacts of convection, lower stratospheric water vapor varies in a similar manner as the observations with coincident peaks and valleys. This suggests that the interannual variability in global lower stratospheric water vapor is largely controlled by processes other than convection, namely by TTL temperatures, as found by many previous studies (Fueglistaler et al., 2009; Randel et al., 2004; Randel & Park, 2019). Thus various modes of climate variability such as ENSO that impact TTL temperatures are important drivers of the interannual variability in lower stratospheric water vapor. Based on the linear correlations between the observed and simulated water vapor time series, we estimate that convection explains approximately 10% (30%) of the total variance in MLS water vapor during winter (summer) over this time period.

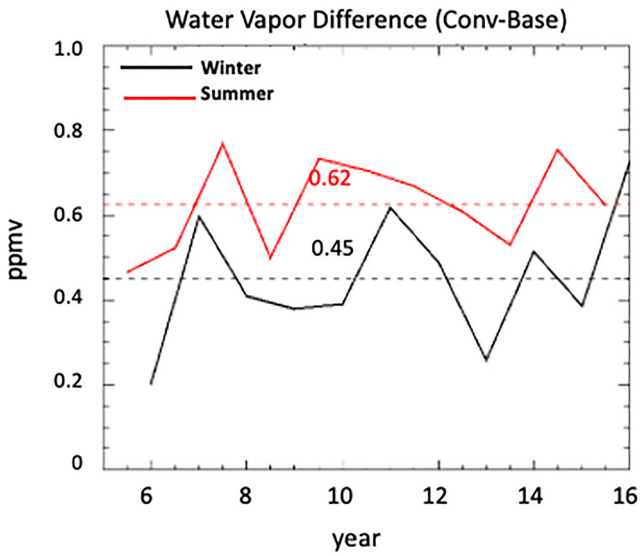


**Figure 7.** Year-to-year variability of the domain-averaged (30°S–30°N for winter, 20°S–50°N for summer) convective impact on the lower stratospheric water vapor mixing ratio during winters (black) and summers (red) 2006–2016. The long-term mean convective impact in the two seasons is shown (in ppmv). Winter is the average of December through February of the year of January, and June through August is represented as the summer value.

The year-to-year variations in the convective impact on the global lower stratospheric water vapor budget are quantified by calculating the water vapor difference fields (i.e., simulation with convection minus simulation without convection) for each season and year. The domain-averaged differences are plotted in a time series for winter and summer separately in Figure 7. When compared to the time series of lower stratospheric water vapor (Figure 6), we find that winters/summers with relatively large convective impact generally correspond to winters/summers with relatively moist stratosphere (e.g., winters 2007, 2011, 2014, and 2016; summers 2007, 2010, and 2014) and vice versa. Overall, the FT model simulations suggest that convection increases water vapor by approximately 0.45 ppmv in winter and 0.62 ppmv in summer, with a standard deviation of 0.15 and 0.10 ppmv, respectively. The amplitudes of the interannual variations in the convective impact in boreal winter and summer are therefore approximately 35% and 17% of their respective means. Recall that we expect the FT model to provide a robust estimate of the relative contribution of convection to the year-to-year variability of lower stratospheric water vapor. Therefore, combining these results with those based on the BT model (i.e., domain-averaged moistening is about 0.3 ppmv), we estimate the impact of convection on the global lower stratospheric water budget to be approximately 0.3 ppmv with year-to-year variations of 0.05–0.1 ppmv during 2006–2016.

## 4. Discussion

The results of this study clearly show that convection reaching the upper troposphere hydrates the lower stratosphere. Convective moistening of the lower stratosphere can occur in basically two ways, as discussed in the Introduction: via (a) the direct injection of water vapor and ice into the lowermost stratosphere and (b) detrainment of ice and subsequent moistening of the tropical uppermost troposphere. Our results based on satellite-derived convective cloud top altitudes suggest the limited role of extreme deep convection overshooting the tropopause on the global lower stratospheric water vapor budget. It is possible that isolated incidences of very deep convective towers are underestimated in our convection product particularly over land areas, given the higher uncertainties in the altitudes (of ∼0.5–1 km) over land compared to over oceanic regions. Nonetheless, the occurrence of deep convection decreases rapidly above ∼400K such that the impact of extreme deep convection on global lower stratospheric water vapor is likely to be small. Given the infrequent occurrence of convective clouds that extend above the tropopause, the primary mechanism of convective moistening of the lower stratosphere is likely through the detrainment of saturated air and ice into the tropical uppermost troposphere. How can moistening of the upper troposphere affect stratospheric water vapor when observations suggest that the stratospheric water vapor mixing ratio is primarily controlled by the cold-point tropopause temperature (e.g., Randel & Park, 2019)?

Aircraft observations in the TTL indicate that low relative humidities occur frequently outside of clouds at temperatures between about 190 and 200K (see fig. 5 in Jensen, Thornberry, et al., 2017). The water vapor mixing ratio of the subsaturated air parcel near the tropopause is primarily determined by moistening and drying events that occur at or below the tropopause. Convection shifts the relative humidity distribution of subsaturated air parcels in the upper troposphere toward higher relative humidity values.

As evidence of this process, Figure 8 shows the relative humidity distribution of FT air parcels in the upper TTL (100 hPa; between 25°S and 25°N) during winter and summer 2010. In both seasons, the relative humidity distribution shifts to higher values for the simulation with convection. The distribution is quite similar to that observed during NASA Airborne Tropical Tropopause Experiment (ATTREX; Jensen, Pfister, et al., 2017), except that the peak at 100% relative humidity is broader and higher in the observations compared to the model. Analysis of parcels in the BT model, which takes into account the detailed cloud microphysical processes in the TTL, indicates that approximately 22% (37%) of convectively influenced parcels during boreal winter (summer) are not subsequently dehydrated by cloud formation before entering the lower stratosphere. These parcels enter the lower stratosphere mainly through the subtropical regions where tropopause temperatures are relatively warm

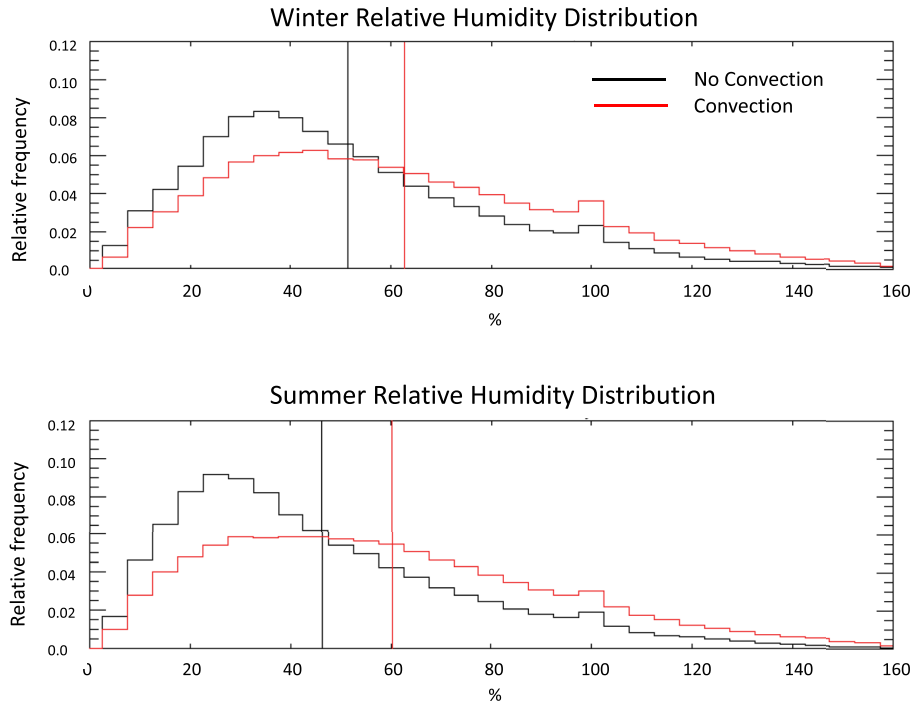


**Figure 8.** Relative humidity distributions of parcels in the forward trajectory model simulations for (top) winter and (bottom) summer 2010: model without convection (black), and model with convection (red). The relative humidity distribution is calculated for parcels at the 100 hPa level between 25°S and 25°N. Vertical lines indicate the mean of each distribution.

(Figure 1) and supersaturation above ∼1.6 is rare. Thus, these parcels not only enhance the relative humidity in the upper TTL, as shown in Figure 8, but they also hydrate the lowermost stratosphere via the upward transport across relatively warm and subsaturated tropopause. While there is interannual variability in upper tropospheric relative humidity, the tendency for convection to shift the relative humidity of upper tropospheric parcels toward higher values is observed consistently from year to year in both seasons.

## 5. Summary and Conclusions

Two complementary modeling approaches are used to investigate the impact of convection on the global lower stratospheric water vapor budget. The BT method provides direct estimates of the water vapor in the global lower stratosphere over a given region and altitude at a given time. The FT method provides a time series of the full three-dimensional water vapor field throughout the stratosphere from a single simulation permitting calculations of the interannual variability of stratospheric water vapor. One of the important differences between the BT and FT model approaches is that the BT model is coupled to a detailed cloud microphysical scheme that properly treats the vertical redistribution of water vapor by ice crystals. We therefore use the BT model to estimate the magnitude of the convective impact during boreal winter and summer 2010, and use the computationally more efficient FT model to examine the relative amplitude of the year-to-year variations in the convective impact. Despite their different approaches, both models simulate the lower stratospheric water vapor field in boreal winter and summer 2010 reasonably well.

The BT model indicates that convection moistens the lower stratosphere by about 0.3 ppmv (0.28 ppmv in winter, 0.32 ppmv in summer), which accounts for approximately 10% of the global lower stratospheric humidity (11% in winter, 9% in summer), in agreement with past studies (e.g., Dauhut & Hohenegger, 2022; Schoeberl et al., 2014; Ueyama et al., 2014, 2015). Convection has a larger (∼1 ppmv or regional mean increase of 30%) impact on the humidity of the lower stratosphere at the 83 hPa level over the Asian summer monsoon region. In both seasons, most of the convective moistening is associated with the rapid saturation of the convectively influenced atmospheric column rather than by the sublimation of convectively detrained ice crystals in aging anvils. Global lower stratospheric humidity exhibits weak sensitivity to small changes in the height of

the global convective cloud tops, including to extreme deep convection overshooting the cold-point tropopause which increases global lower stratospheric humidity by only 1% in both seasons. We note that the impact of overshooting convection may be underestimated in this study due to limitations of our methodology such as the focus on the water vapor effect at 83 hPa level only as well as the lack of mixing above the overshooting cloud top (Dauhut et al., 2018; Lane, 2008). The diurnal peak in convection accounts for about half of the total convective moistening of the lower stratosphere during winter and nearly all of the convective moistening during summer.

Simulations with the FT model show that the interannual variability in global lower stratospheric water vapor during 2006–2016 is largely controlled by processes other than convection (i.e., TTL temperatures). Convection contributes between 0.05 and 0.1 ppmv of the year-to-year variability in stratospheric water vapor. Years with relatively large convective impact generally correspond to years with relatively moist stratosphere, and vice versa. Combining the FT model results with those based on the BT model, we estimate the impact of convection on the global lower stratospheric water vapor budget to be a moistening of approximately 0.3 ppmv with year-to-year variations of up to 0.1 ppmv during 2006–2016.

Analyses of parcel relative humidities in the FT model show that convection in the upper troposphere shifts the relative humidity distribution of upper tropospheric parcels toward higher humidities. A significant fraction (i.e., up to about a third) of these parcels in the upper troposphere with high relative humidities do not undergo ice nucleation during their ascent, and ultimately increase the globally averaged stratospheric water vapor. In other words, the dominant mechanism of convective hydration of the lower stratosphere appears to be via the detrainment of saturated air and ice into the tropical uppermost troposphere, followed by ascent into the stratosphere. Extreme deep convection overshooting the tropopause, which is rare relative to convection reaching the upper troposphere, has relatively small impact on the global lower stratospheric water vapor budget.

In summary, the impact of convection on the global lower stratospheric water vapor budget is relatively small in the current climate, although it can be much larger on a regional basis such as over the summer monsoon regions. Our results suggest that a convective impact on the global lower stratospheric humidity of more than 10% would require significant changes in global convective activity from the current climate. Nonetheless, as the summer monsoon anticyclone and convection have been shown to substantially influence the distribution of trace gases in the UTLS (Dethof et al., 1999; Garny & Randel, 2016; Gettelman et al., 2004; Jensen et al., 2020; Orbe et al., 2015; Pan et al., 2016; Randel et al., 2012; Randel & Park, 2006; Santee et al., 2017; Schwartz et al., 2013; Smith et al., 2017), a significant change in monsoon convection and/or cirrus cloud distribution in future climate could potentially have a measurable effect on the composition of the stratosphere.

## Data Availability Statement

All data used in this study are publicly available at no charge and with unrestricted access. The satellite-derived convective cloud top altitude data set (Pfister et al., 2022) is available at https://bocachica.arc.nasa.gov/nasaarc_cldalt/. The Aura MLS water vapor v5.0 data (Lambert et al., 2020; Livesey et al., 2020) are available through the NASA Goddard Earth Sciences Data and Information Center (GES DISC) at https://dx.doi.org/10.5067/Aura/MLS/DATA2508. The fifth generation of European Centre for Medium-range Weather Forecast reanalysis data (ERA5; Hersbach et al., 2020) are available through the Climate Data Store web interface at https://doi.org/10.24381/cds.bd0915c6. The Modern-Era Retrospective Analysis for Research and Applications, Version 2 (MERRA-2) reanalysis data (Gelaro et al., 2017) are obtained from the Global Modeling and Assimilation Office (GMAO), *inst3*_3d_*asm_Cp: MERRA-2 3D IAU State, Meteorology Instantaneous 3-hourly (p-coord, 0.625x0.5L42), version 5.12.4* at https://doi.org/10.5067/WWQSXQ8IVFW8. The 2B-FLXHR-LIDAR version R05 heating rate data (Henderson et al., 2013; L'Ecuyer et al., 2008) used for diabatic trajectory calculations are available through the CloudSat Data Processing Center at https://www.cloudsat.cira.colostate.edu/data-products/2b-flxhr-lidar. Analyses were done and figures were made with IDL (Interactive Data Language) software from L3Harris Geospatial (https://www.l3harrisgeospatial.com/Software-Technology/IDL) licensed to Rei Ueyama at NASA Ames Research Center.

**Acknowledgments**
The authors would like to thank three anonymous reviewers for their comments on the manuscript. This work is supported by NASA grants in the Upper Atmospheric Composition Observations and Aura Science Team (Grant 80NSSC20K1235) programs as well as with funding from the Earth Venture Suborbital (EVS-3) Dynamics and Chemistry of the Summer Stratosphere (DCOTSS) project. RU is also supported by the Atmospheric Composition Program through the NASA Internal Scientist Funding Model. The National Center for Atmospheric Research is operated by the University Corporation for Atmospheric Research, under sponsorship of the National Science Foundation.

## References

Adler, R. F., & Mack, R. A. (1986). Thunderstorm cloud top dynamics as inferred from satellite observations and a cloud top parcel model. *Journal of the Atmospheric Sciences*, *43*(18), 1945–1960. https://doi.org/10.1175/1520-0469(1986)043<1945:TCTDAI>2.0.CO;2

Anderson, J. G., Wilmouth, D. M., Smith, J. B., & Sayres, D. S. (2012). UV dosage levels in summer: Increased risk of ozone loss from convectively injected water vapor. *Science*, *337*(6096), 835–839. https://doi.org/10.1126/science.1222978

Avery, M. A., Davis, S. M., Rosenlof, K. H., Ye, H., & Dessler, A. E. (2017). Large anomalies in lower stratospheric water vapour and ice during the 2015-2016 El Niño. *Nature Geoscience*, *10*(6), 405–409. https://doi.org/10.1036/ngeo2961

Banerjee, A., Chiodo, G., Previdi, M., Ponater, M., Conley, A. J., & Polvani, L. M. (2019). Stratospheric water vapor: An important climate feedback. *Climate Dynamics*, *53*(3–4), 1697–1710. https://doi.org/10.1007/s00382-019-04721-4

Bergman, J. W., Jensen, E. J., Pfister, L., & Yang, Q. (2012). Seasonal differences of vertical-transport efficiency in the tropical tropopause layer: On the interplay between tropical deep convection, large-scale vertical ascent, and horizontal circulations. *Journal of Geophysical Research: Atmospheres*, *117*(D5), D05302. https://doi.org/10.1029/2011JD016992

Boehm, M. T., & Verlinde, J. (2000). Stratospheric influence on upper tropospheric tropical cirrus. *Geophysical Research Letters*, *27*(19), 3209–3212.

Bowman, K. P. (1993). Large-scale isentropic mixing properties of the Antarctic polar vortex from analyzed winds. *Journal of Geophysical Research*, *98*(D12), 23013–23027. https://doi.org/10.1029/93JD02599

Bowman, K. P., & Carrie, G. D. (2002). The mean-meridional transport circulation of the troposphere in an idealized GCM. *Journal of the Atmospheric Sciences*, *59*(9), 1502–1514. https://doi.org/10.1175/1520-0469(2002)059<1502:TMMTCO>2.0.CO;2

Brewer, A. W. (1949). Evidence for a world circulation provided by the measurements of helium and water vapor distribution in the stratosphere. *Quarterly Journal of the Royal Meteorological Society*, *75*(326), 351–363. https://doi.org/10.1002/qj.49707532603

Chae, J. H., Wu, D. L., Read, W. G., & Sherwood, S. C. (2011). The role of tropical deep convective clouds on temperature, water vapor, and dehydration in the tropical tropopause layer (TTL). *Atmospheric Chemistry and Physics*, *11*(8), 3811–3821. https://doi.org/10.5194/acp-11-3811-2011

Chang, K.-W., & L'Ecuyer, T. (2020). Influence of gravity wave temperature anomalies and their vertical gradients on cirrus clouds in the tropical tropopause layer – A satellite-based view. *Atmospheric Chemistry and Physics*, *20*(21), 12499–12514. https://doi.org/10.5194/acp-20-12499-2020

Chou, C., & Chen, C.-A. (2010). Depth of convection and the weakening of tropical circulation in global warming. *Journal of Climate*, *23*(11), 3019–3030. https://doi.org/10.1175/2010JCLI3383.1

Corti, T., Luo, B. P., de Reus, M., Brunner, D., Cairo, F., Mahoney, M. J., et al. (2008). Unprecedented evidence for deep convection hydrating the tropical stratosphere. *Geophysical Research Letters*, *35*(10), L10810. https://doi.org/10.1029/2008GL033641

Danielsen, E. F. (1982). A dehydration mechanism for the stratosphere. *Geophysical Research Letters*, *9*(6), 605–608. https://doi.org/10.1029/GL009i006p00605

Danielsen, E. F. (1983). In situ evidence of rapid, vertical, irreversible transport of lower tropospheric air into the lower tropical stratosphere by convective cloud turrets and by larger-scale upwelling in tropical cyclones. *Journal of Geophysical Research: Atmospheres*, *98*(D5), 8665–8681. https://doi.org/10.1029/92JD02954

Dauhut, T., Chaboureau, J.-P., Haynes, P. H., & Lane, T. P. (2018). The mechanisms leading to a stratospheric hydration by overshooting convection. *Journal of the Atmospheric Sciences*, *75*(12), 4383–4398. https://doi.org/10.1175/JAS-D-18-0176.1

Dauhut, T., & Hohenegger, C. (2022). The contribution of convection to the stratospheric water vapor: The first budget using a global storm-resolving model. *Journal of Geophysical Research: Atmospheres*, *127*(5), e2021JD036295. https://doi.org/10.1029/2021JD036295

Dessler, A. E., Schoeberl, M. R., Wang, T., Davis, S. M., & Rosenlof, K. H. (2013). Stratospheric water vapor feedback. *Proceedings of the National Academy of Sciences of the United States of America*, *110*(45), 18087–18091. https://doi.org/10.1073/pnas.1310344110

Dessler, A. E., Schoeberl, M. R., Wang, T., Davis, S. M., Rosenlof, K. H., & Vernier, J.-P. (2014). Variations of stratospheric water vapor over the past three decades. *Journal of Geophysical Research: Atmospheres*, *119*(22), 12588–12598. https://doi.org/10.1002/2014JD021712

Dessler, A. E., Ye, H., Wang, T., Schoeberl, M. R., Oman, L. D., Douglass, A. R., et al. (2016). Transport of ice into the stratosphere and the humidification of the stratosphere over the 21st century. *Geophysical Research Letters*, *43*(5), 2323–2329. https://doi.org/10.1002/2016GL067991

Dethof, A., O'Neill, A., Slingo, J. M., & Smit, H. G. J. (1999). A mechanism for moistening the lower stratosphere involving the Asian summer monsoon. *Quarterly Journal of the Royal Meteorological Society*, *125*(556), 1079–1106. https://doi.org/10.1002/qj.1999.49712555602

Dinh, T., Podglajen, A., Hertzog, A., Legras, B., & Plougonven, R. (2016). Effect of gravity wave temperature fluctuations on homogeneous ice nucleation in the tropical tropopause layer. *Atmospheric Chemistry and Physics*, *16*(1), 35–46. https://doi.org/10.5194/acp-16-35-2016

Dvortsov, V. L., & Solomon, S. (2001). Response of the stratospheric temperatures and ozone to past and future increase in stratospheric humidity. *Journal of Geophysical Research: Atmospheres*, *106*(D7), 7505–7514. https://doi.org/10.1029/2000JD900637

Forster, P. M. F., & Shine, K. P. (1999). Stratospheric water vapor changes as a possible contributor to observed stratospheric cooling. *Geophysical Research Letters*, *26*(21), 3309–3312. https://doi.org/10.1029/1999GL010487

Forster, P. M. F., & Shine, K. P. (2002). Assessing the climate impact of trends in stratospheric water vapor. *Geophysical Research Letters*, *29*(6), 101–104. https://doi.org/10.1029/2001GL013909

Frey, W., Borrmann, S., Fierli, F., Weigel, R., Miev, V., Matthey, R., et al. (2014). Tropical deep convective life cycle: Cb-anvil cloud microphysics from high-altitude aircraft observations. *Atmospheric Chemistry and Physics*, *14*(23), 13223–13240. https://doi.org/10.5194/acp-14-13223-2014

Frey, W., Borrmann, S., Kunkel, D., Weigel, R., de Reus, M., Schlager, H., et al. (2011). In situ measurements of tropical cloud properties in the West African monsoon: Upper tropospheric ice clouds, mesoscale convective system outflow, and subvisual cirrus. *Atmospheric Chemistry and Physics*, *11*(12), 5569–5590. https://doi.org/10.5194/acp-11-5569-2011

Frey, W., Schofield, R., Hoor, P., Kunkel, D., Ravegnani, F., Ulanovsky, A., et al. (2015). The impact of overshooting deep convection on local transport and mixing in the tropical upper troposphere/lower stratosphere (UTLS). *Atmospheric Chemistry and Physics*, *15*(11), 6467–6486. https://doi.org/10.5194/acp-15-6467-2015

Fueglistaler, S., & Baker, M. B. (2006). A modelling study of the impact of cirrus clouds on the moisture budget of the upper troposphere. *Atmospheric Chemistry and Physics*, *6*(5), 1425–1434. https://doi.org/10.5194/acp-6-1425-2006

Fueglistaler, S., Bonazzola, M., Haynes, P. H., & Peter, T. (2005). Stratospheric water vapor predicted from the Lagrangian temperature history of air entering the stratosphere in the tropics. *Journal of Geophysical Research*, *110*(D8), D08107. https://doi.org/10.1029/2004JD005516

Fueglistaler, S., Dessler, A. E., Dunkerton, T. J., Folkins, I., Fu, Q., & Mote, P. W. (2009). Tropical tropopause layer. *Reviews of Geopohysics*, *47*(1), RG1004. https://doi.org/10.1029/2008RG00267

Fujiwara, M., Iwasaki, S., Shimizu, A., Inai, Y., Shiotani, M., Hasebe, F., et al. (2009). Cirrus observations in the tropical tropopause layer over the western Pacific. *Journal of Geophysical Research: Atmospheres*, *114*(D9), D09304. https://doi.org/10.1029/2008JD011040

Garny, H., & Randel, W. J. (2016). Transport pathways from the Asian monsoon anticyclone to the stratosphere. *Atmospheric Chemistry and Physics*, *16*(4), 2703–2718. https://doi.org/10.5194/acp-16-2703-2016

Garrett, T. J., Dean-Day, J., Liu, C., Barnett, B., Mace, G., Baumgardner, D., et al. (2006). Convective formation of pileus cloud near the tropopause. *Atmospheric Chemistry and Physics*, *6*(5), 1185–1200. https://doi.org/10.5194/acp-6-1185-2006

Garrett, T. J., Heymsfield, A. J., McGill, M. J., Ridley, B. A., Baumgardner, D. G., Bui, T. P., & Webster, C. R. (2004). Convective generation of cirrus near the tropopause. *Journal of Geophysical Research: Atmospheres*, *109*(D21), D21203. https://doi.org/10.1029/2004JD004952

Gasparini, B., Blossey, P. N., Hartmann, D. L., Lin, G., & Fan, J. (2019). What drives the life cycle of tropical anvil clouds? *Journal of Advances in Modeling Earth Systems*, *11*(8), 2586–2605. https://doi.org/10.1029/2019MS001736

Gelaro, R., McCarty, W., Suárez, M. J., Todling, R., Molod, A., Takacs, L., et al. (2017). The Modern-Era Retrospective Analysis for Research and Applications, Version 2 (MERRA-2) [Dataset]. Journal of Climate, *30*(14), 5419–5454. https://doi.org/10.1175/JCLI-D-16-0758.1

Gettelman, A., Kinnison, D. E., Dunkerton, T. J., & Brasseur, G. P. (2004). Impact of monsoon circulations on the upper troposphere and lower stratosphere. *Journal of Geophysical Research: Atmospheres*, *109*(D22), D22101. https://doi.org/10.1029/2004JD004878

Gettelman, A., Salby, M. L., & Sassi, F. (2002). Distribution and influence of convection in the tropical tropopause region. *Journal of Geophysical Research: Atmospheres*, *107*(D10), ACL6-1–ACL6-12. https://doi.org/10.1029/2001JD001048

Griffin, S., Bedka, K., & Velden, C. (2016). A method for calculating the height of overshooting convective cloud tops using satellite-based IR imager and CloudSat cloud profiling radar observations. *Journal of Applied Meteorology and Climatology*, *55*(2), 479–491. https://doi.org/10.1175/JAMC-D-15-0170.1

Hartmann, D. L., Holton, J. R., & Fu, Q. (2001). The heat balance of the tropica tropopause, cirrus, and stratospheric dehydration. *Geophysical Research Letters*, *28*(10), 1969–1972. https://doi.org/10.1029/2000GL012833

Hassim, M. E. E., & Lane, T. P. (2010). A model study on the influence of overshooting convection on TTL water vapour. *Atmospheric Chemistry and Physics*, *10*(20), 9833–9849. https://doi.org/10.5194/acp-10-9833-2010

Hatsushika, H., & Yamazaki, K. (2003). Stratospheric drain over Indonesia and dehydration within the tropical tropopause layer diagnosed by air parcel trajectories. *Journal of Geophysical Research: Atmospheres*, *108*(D19), 4610. https://doi.org/10.1029/2002JD002986

Held, I. M., & Soden, B. J. (2006). Robust responses of the hydrological cycle to global warming. *Journal of Climate*, *19*(21), 5686–5699. https://doi.org/10.1175/JCLI3990.1

Henderson, D. S., L'Ecuyer, T., Stephens, G., Partain, P., & Sekiguchi, M. (2013). A multisensory perspective on the radiative impacts of clouds and aerosols [Dataset]. Journal of Applied Meteorology and Climatology, *52*(4), 853–871. https://doi.org/10.1175/JAMC-D-12-025.1

Hersbach, H., Bell, B., Berrisford, P., Hirahara, S., Horányi, A., Muñoz-Sabater, J., et al. (2020). The ERA5 global reanalysis [Dataset]. Quarterly Journal of the Royal Meteorological Society, *146*(730), 1999–2049. https://doi.org/10.1002/qj.3803

Holton, J. R., & Gettelman, A. (2001). Horizontal transport and the dehydration of the stratosphere. *Geophysical Research Letters*, *28*(14), 2799–2802. https://doi.org/10.1029/2001GL013148

Holton, J. R., Haynes, P. H., McIntyre, M. E., Douglass, A. R., Rood, R. B., & Pfister, L. (1995). Stratosphere-troposphere exchange. *Reviews of Geopohysics*, *33*(4), 403–439. https://doi.org/10.1029/95RG02097

Homeyer, C. R., McAuliffe, J. D., & Bedka, K. M. (2017). On the development of above-anvil cirrus plumes in extratropical convection. *Journal of the Atmospheric Sciences*, *74*(5), 1617–1633. https://doi.org/10.1175/JAS-D-16-0269.1

Huang, Y., Wang, Y., & Huang, H. (2020). Stratospheric water vapor feedback disclosed by a locking experiment. *Geophysical Research Letters*, *47*(12), e2020GL087987. https://doi.org/10.1029/2020GL087987

Huffman, G., Bolvin, D., Nelkin, E., Wolff, D., Adler, R., Gu, G., et al. (2007). The TRMM Multisatellite Precipitation Analysis (TMPA): Quasi-global, multiyear, combined-sensor precipitation estimates at fine scales. *Journal of Hydrometeorology*, *8*(1), 38–55. https://doi.org/10.1175/JHM560.1

Huffman, G., Stoker, E., Bolvin, D., Nelkin, E., & Tan, J. (2019). *GPM IMERG final precipitation L3 1 day 0.1 degree x 1 degree V06*. In A. Savtchenko, & M. D. Greenbelt (Eds.), Goddard Earth Sciences Data and Information Services Center (GES DISC). https://doi.org/10.5067/GPM/IMERGDF/DAY/06

Hurst, D. F., Read, W. G., Vömel, H., Selkirk, H. B., Rosenlof, K. H., Davis, S. M., et al. (2016). Recent divergences in stratospheric water vapor measurements by frost point hygrometers and the Aura Microwave Limb Sounder. *Atmospheric Measurement Techniques*, *9*, 4447–4457. https://doi.org/10.5194/amt-9-4447-2016

Immler, F., Krüger, K., Fujiwara, M., Verver, G., Rex, M., & Schrems, O. (2008). Correlation between equatorial Kelvin waves and the occurrence of extremely thin ice clouds at the tropical tropopause. *Atmospheric Chemistry and Physics*, *8*(14), 4019–4026. https://doi.org/10.5194/acp-8-4019-2008

Jensen, E. J., Lawson, P., Baker, B., Pilson, B., Mo, Q., Heymsfield, A. J., et al. (2009). On the importance of small ice crystals in tropical anvil cirrus. *Atmospheric Chemistry and Physics*, *9*(15), 5519–5537. https://doi.org/10.5194/acp-9-5519-2009

Jensen, E. J., Pan, L. L., Honomichl, S., Diskin, G. S., Krämer, M., Spelten, N., et al. (2020). Assessment of observational evidence for direct convective hydration of the lower stratosphere. *Journal of Geophysical Research: Atmospheres*, *125*(15), e2020JD032793. https://doi.org/10.1029/2020JD032793

Jensen, E. J., & Pfister, L. (2004). Transport and freeze-drying in the tropical tropopause layer. *Journal of Geophysical Research*, *109*(D2), D02207. https://doi.org/10.1029/2003JD004022

Jensen, E. J., Pfister, L., Jordan, D. E., Bui, T. V., Ueyama, R., Singh, H. B., et al. (2017). The NASA Airborne tropical tropopause experiment: High-altitude aircraft measurements in the Tropical Western Pacific. *Bulletin of the American Meteorological Society*, *98*(1), 129–143. https://doi.org/10.1175/BAMS-D-14-00263.1

Jensen, E. J., Pfister, L., & Toon, O. B. (2011). Impact of radiative heating, wind shear, temperature variability, and microphysical processes on the structure and evolution of thin cirrus in the tropical tropopause layer. *Journal of Geophysical Research*, *116*(D12), D12209. https://doi.org/10.1029/2010JD015417

Jensen, E. J., Thornberry, T. D., Rollins, A. W., Ueyama, R., Pfister, L., Bui, T., et al. (2017). Physical processes controlling the spatial distributions of relative humidity in the tropical tropopause layer over the Pacific. *Journal of Geophysical Research: Atmospheres*, *122*(11), 6094–6107. https://doi.org/10.1002/2017JD026632

Kärcher, B., Hendricks, J., & Lohmann, U. (2006). Physically based parameterization of cirrus cloud formation for use in global atmospheric models. *Journal of Geophysical Research: Atmospheres*, *111*(D1), D01205. https://doi.org/10.1029/2005JD006219

Kelly, K. K., Proffitt, M. H., Chan, K. R., Loewenstein, M., Podolske, J. R., Strahan, S. E., et al. (1993). Water vapor and cloud water measurements over Darwin during the STEP 1987 tropical mission. *Journal of Geophysical Research*, *98*(D5), 8713–8723. https://doi.org/10.1029/92JD02526

Kiehl, J. T., & Solomon, S. (1986). On the radiative balance of the stratosphere. *Journal of the Atmospheric Sciences*, *43*(14), 1525–1534. https://doi.org/10.1175/1520-0469(1986)043<1525:OTRBOT>2.0.CO;2

Kim, J., Randel, W. J., & Birner, T. (2018). Convectively driven tropopause-level cooling and its influences on stratospheric moisture. *Journal of Geophysical Research: Atmospheres*, *123*(1), 590–606. https://doi.org/10.1029/2017JD027080

Kim, J.-E., Alexander, M. J., Bui, T. P., Dean-Day, J. M., Lawson, R. P., Woods, S., et al. (2016). Ubiquitous influence of waves on tropical high cirrus clouds. *Geophysical Research Letters*, *43*(11), 5895–5901. https://doi.org/10.1029/2016GL069293

Koop, T., Luo, B., Tsias, A., & Peter, T. (2000). Water activity as the determinant for homogeneous ice nucleation in aqueous solutions. *Nature*, *406*(6796), 611–614. https://doi.org/10.1038/35020537

Krämer, M., Rolf, C., Spelten, N., Afchine, A., Fahey, D., Jensen, E., et al. (2020). A microphysics guide to cirrus – Part 2: Climatologies of clouds and humidity from observations. *Atmospheric Chemistry and Physics*, *20*(21), 12569–12608. https://doi.org/10.5194/acp-20-12569-2020

Kritz, M. A., Rosner, S. W., Kelly, K. K., Loewenstein, M., & Chan, K. R. (1993). Radon measurements in the lower tropical stratosphere: Evidence for rapid vertical transport and dehydration of tropospheric air. *Journal of Geophysical Research: Atmospheres*, *98*(D5), 8725–8736. https://doi.org/10.1029/92JD02524

Lambert, A., Read, W., & Livesey, N. (2015). *MLS/Aura level2 water vapor (H2O) mixing ratio V004*. Goddard Earth Sciences Data and Information Services Center (GES DISC)

Lambert, A., Read, W., & Livesey, N. (2015). *MLS/Aura level2 water vapor (H2O) mixing ratio V004*. Goddard Earth Sciences Data and Information Services Center (GES DISC).

Lane, T. (2008). The vortical response to penetrative convection and the associated gravity-wave generation. *Atmospheric Science Letters*, *9*(3), 103–110. https://doi.org/10.1002/asl.167

L'Ecuyer, T. S., Wood, N. B., Haladay, T., Stephens, G. L., & Stackhouse Jr., P. W. (2008). Impact of clouds on atmospheric heating based on the R04 CloudSat fluxes and heating rates data set [Dataset]. Journal of Geophysical Research, *113*, D00A15. https://doi.org/10.1029/2008JD009951

Lee, K.-O., Dauhut, T., Chaboureau, J.-P., Khyaykin, S., Krämer, M., & Rolf, C. (2019). Convective hydration in the tropical tropopause layer during the StratoClim aircraft campaign: Pathway of an observed hydration patch. *Atmospheric Chemistry and Physics*, *19*(18), 11803–11820. https://doi.org/10.5194/acp-19-11803-2019

Li, F., & Newman, P. (2020). Stratospheric water vapor feedback and its climate impacts in the coupled atmosphere-ocean Goddard Earth Observing System Chemistry-Climate Model. *Climate Dynamics*, *55*(5–6), 1585–1595. https://doi.org/10.1007/s00382-020-05348-6

Liu, C., & Zipser, E. J. (2005). Global distribution of convection penetrating the tropical tropopause. *Journal of Geophysical Research: Atmospheres*, *110*(D23), D23104. https://doi.org/10.1029/2005JD006063

Liu, N., & Liu, C. (2016). Global distribution of deep convection reaching tropopause in 1 year GPM observations. *Journal of Geophysical Research: Atmospheres*, *121*(8), 3824–3842. https://doi.org/10.1002/2015JD024430

Livesey, N. J., Read, W. G., Froidevaux, L., Lambert, A., Santee, M. L., Schwartz, M. J., et al. (2021). Investigation and amelioration of long-term instrumental drifts in water vapor and nitrous oxide measurements from the Aura Microwave Limb Sounder (MLS) and their implications for studies of variability and trends. *Atmosospheric Chemistry and Physics*, *21*(20), 15409–15430. https://doi.org/10.5194/acp-21-15409-2021

Livesey, N. J., Read, W. G., Wagner, P. A., Froidevaux, L., Santee, M. L., Schwartz, M. J., et al. (2020). Version 5.0x Level 2 and 3 data quality and description document (Tech. Rep. No. JPL D-105336 Rev. B) [Dataset]. Jet Propulsion Laboratory, Retrieved from https://mls.jpl.nasa.gov/data/v5-0_data_quality_document.pdf

Maycock, A. C., Joshi, M. M., Shine, K. P., & Scaife, A. A. (2013). The circulation response to idealized changes in stratospheric water vapor. *Journal of Climate*, *26*(2), 454–561. https://doi.org/10.1175/JCLI-D-12-00155.1

Minnis, P., Yost, C., Sun-Mack, S., & Chen, Y. (2008). Estimating the top altitude of optically thick ice clouds from thermal infrared satellite observations using CALIPSO data. *Geophysical Research Letters*, *35*(12), L12801. https://doi.org/10.1029/2008GL033947

Mote, P. W., Rosenlof, K. H., McIntyre, M. E., Carr, E. S., Gille, J. C., Holton, J. R., et al. (1996). An atmospheric tape-recorder: The imprint of tropical tropopause temperatures on stratospheric water vapor. *Journal of Geophysical Research*, *101*(D2), 3989–4006. https://doi.org/10.1029/95JD03422

Nielsen, J. K., Larsen, N., Cairo, F., Di Donfrancesco, G., Rosen, J. M., Durry, G., et al. (2007). Solid particles in the tropical lowest stratosphere. *Atmospheric Chemistry and Physics*, *7*(3), 685–695. https://doi.org/10.5194/acp-7-685-2007

Orbe, C., Waugh, D. W., & Newman, P. A. (2015). Air-mass origin in the tropical lower stratosphere: The influence of Asian boundary layer air. *Geophysical Research Letters*, *42*(10), 4240–4248. https://doi.org/10.1002/2015GL063937

Pan, L. L., Honomichl, S. B., Kinnison, D. E., Abalos, M., Randel, W. J., Bergman, J. W., et al. (2016). Transport of chemical tracers from the boundary laer to stratosphere associated with the dynamics of the Asian summer monsoon. *Journal of Geophysical Research: Atmospheres*, *121*(23), 14159–14174. https://doi.org/10.1029/2016JD025616

Pfister, L., Ueyama, R., Jensen, E. J., & Schoeberl, M. R. (2022). Evaluating deep convective cloud top altitudes at high temporal and spatial resolution [Dataset]. Earth and Space Science, *9*(11), https://doi.org/10.1029/2022ea002475, Manuscript in final review.

Pfister, L., Chan, K. R., Bui, T. P., Bowen, S., Legg, M., Gary, B., et al. (1993). Gravity waves generated by a tropical cyclone during the STEP tropical field program: A case study. *Journal of Geophysical Research*, *98*(D5), 8611–8638. https://doi.org/10.1029/92JD01679

Poshyvailo, L., Müller, R., Konopka, P., Günther, G., Riese, M., Podglajen, A., & Ploeger, F. (2018). Sensitivities of modelled water vapour in the lower stratosphere: Temperature uncertainty, effects of horizontal transport and small-scale mixing. *Atmosospheric Chemistry and Physics*, *18*(12), 8505–8527. https://doi.org/10.5194/acp-18-8508-2018

Potter, B. E., & Holton, J. R. (1995). The role of monsoon convection in the dehydration of the lower tropical stratosphere. *Journal of the Atmospheric Sciences*, *52*(8), 1034–1050. https://doi.org/10.1175/1520-0469(1995)052<1034:TROMCI>2.0.CO;2

Randel, W. J., & Jensen, E. J. (2013). Physical processes in the tropical tropopause layer and their roles in a changing climate. *Nature Geoscience*, *6*(3), 169–176. https://doi.org/10.1038/ngeo1733

Randel, W. J., Moyer, E., Park, M., Jensen, E. J., Bernath, P., Walker, K., & Boone, C. (2012). Global variations of HDO and HDO/$H_2O$ ratios in the upper troposphere and lower stratosphere derived from ACE-FTS satellite measurements. *Journal of Geophysical Research: Atmospheres*, *117*(D6), D06303. https://doi.org/10.1029/2011JD016632

Randel, W. J., & Park, M. (2006). Deep convective influence on the Asian summer monsoon anticyclone and associated tracer variability observed with Atmospheric Infrared Sounder (AIRS). *Journal of Geophysical Research: Atmospheres*, *111*(D12), D12314. https://doi.org/10.1029/2005JD006490

Randel, W. J., & Park, M. (2019). Diagnosing observed stratospheric water vapor relationships to the cold point tropical tropopause. *Journal of Geophysical Research: Atmospheres*, *124*(13), 7018–7033. https://doi.org/10.1029/2019JD030648

Randel, W. J., & Wu, F. (2015). Variability of zonal mean tropical temperatures derived from a decade of GPS radio occultation data. *Journal of the Atmospheric Sciences*, *72*(3), 1261–1275. https://doi.org/10.1175/JAS-D-14-0216.1

Randel, W. J., Wu, F., Oltmans, S. J., Rosenlof, K., & Nedoluha, G. E. (2004). Interannual changes of stratospheric water vapor and correlations with tropical tropopause temperatures. *Journal of the Atmospheric Sciences*, *61*(17), 2133–2148. https://doi.org/10.1175/1520-0469(2004)061<2133:ICOSWV>2.0.CO;2

Randel, W. J., Zhang, K., & Fu, R. (2015). What controls stratospheric water vapor in the NH summer monsoon regions? *Journal of Geophysical Research: Atmospheres*, *120*(15), 7988–8001. https://doi.org/10.1002/2015JD023622

Reinares Martinez, I., Evan, S., Wienhold, G., Brioude, J., Jensen, E. J., Thornberry, T. D., et al. (2021). Unprecedented observations of a nascent in situ cirrus in the tropical tropopause layer. *Geophysical Research Letters*, *48*(4), e2020GL090936. https://doi.org/10.1029/2020GL090936

Robinson, F. J., & Sherwood, S. C. (2006). Modeling the impact of convective entrainment on the tropical tropopause. *Journal of the Amotphseric Sciences*, *63*(3), 1013–1027. https://doi.org/10.1175/JAS3673.1

Romps, D. M. (2011). Response of tropical precipitation to global warming. *Journal of the Atmosphseric Sciences*, *68*(1), 123–138. https://doi.org/10.1175/2010JAS3542.1

Salby, M., & Callagha, P. (2004). Control of the tropical tropopause and vertical transport across it. *Journal of Climate*, *17*(5), 965–985. https://doi.org/10.1175/1520-0442(2004)017<0965:COTTTA>2.0CO;2

Santee, M. L., Manney, G. L., Livesey, N. J., Schwartz, M. J., Neu, J. L., & Read, W. G. (2017). A comprehensive overview of the climatological composition of the Asian summer monsoon anticyclone based on 10 years of Aura Microwave Limb Sounder measurements. *Journal of Geophysical Research: Atmospheres*, *122*(10), 5491–5514. https://doi.org/10.1029/2016JD026408

Schneider, E. K., Kirtman, B. P., & Lindzen, R. S. (1999). Tropospheric water vapor and climate sensitivity. *Journal of the Amotphseric Sciences*, *56*(11), 1649–1658. https://doi.org/10.1175/1520-0469(1999)056<1649:TWVACS>2.0.CO;2

Schoeberl, M. R., & Dessler, A. E. (2011). Dehydration of the stratosphere. *Atmospheric Chemistry and Physics*, *11*(16), 8433–8446. https://doi.org/10.5194/acp-11-8433-2011

Schoeberl, M. R., Dessler, A., Wang, T., Avery, M., & Jensen, E. J. (2014). Cloud formation, convection, and stratospheric dehydration. *Earth and Space Science*, *1*, 1–17. https://doi.org/10.1002/2014EA000014

Schoeberl, M. R., Dessler, A., Ye, H., Wang, T., Avery, M., & Jensen, E. (2016). The impact of gravity waves and cloud nucleation threshold on stratospheric water and tropical tropospheric cloud fraction. *Earth and Space Science*, *3*(8), 295–305. https://doi.org/10.1002/2016EA000180

Schoeberl, M. R., Douglass, A. R., Stolarski, R. S., Pawson, S., Strahan, S. E., & Read, W. (2008). Comparison of lower stratospheric tropical mean vertical velocities. *Journal of Geophysical Research*, *113*(D24), D24109. https://doi.org/10.1029/2008JD010221

Schoeberl, M. R., Jensen, E. J., Pfister, L., Ueyama, R., Avery, M., & Dessler, A. (2018). Convective hydration of the upper troposphere and lower stratosphere. *Journal of Geophysical Research: Atmospheres*, *123*(9), 4583–4593. https://doi.org/10.1029/2018JD028286

Schoeberl, M. R., Jensen, E. J., Pfister, L., Ueyama, R., Wang, T., & Selkirk, H. (2019). Water vapor, clouds, and saturation in the tropical tropopause layer. *Journal of Geophysical Research: Atmospheres*, *124*(7), 3984–4003. https://doi.org/10.1029/2018JD029849

Schoeberl, M. R., Jensen, E. J., Podglajen, A., Coy, L., Candido, S., & Carver, R. (2017). Gravity wave spectra in the lower stratosphere diagnosed from project loon balloon trajectories. *Journal of Geophysical Research: Atmospheres*, *122*(16), 8517–8524. https://doi.org/10.1002/2017JD026471

Schoeberl, M. R., Jensen, E. J., & Woods, S. (2015). Gravity waves amplify upper tropospheric dehydration by clouds. *Earth and Space Science*, *2*(12), 485–500. https://doi.org/10.1002/2015EA000127

Schwartz, M. J., Read, W. G., Santee, M. L., Livesey, N. J., Froidevaux, L., Lambert, A., & Manney, G. L. (2013). Convectively injected water vapor in the North American summer lowermost stratosphere. *Geophysical Research Letters*, *40*(10), 2316–2321. https://doi.org/10.1002/grl.50421

Selkirk, H. B. (1993). The tropopause cold trap in the Australian monsoon during STEP/AMEX 1987. *Journal of Geophysical Research: Atmospheres*, *98*(D5), 8591–8610. https://doi.org/10.1029/92JD02932

Sherwood, S. C., Chae, J., Minnis, P., & McGill, M. (2004). Underestimation of deep convective cloud tops by thermal imagery. *Geophysical Research Letters*, *31*(11), L11102. https://doi.org/10.1029/2004GL019699

Sherwood, S. C., & Dessler, A. (2000). On the control of stratospheric humidity. *Geophysical Research Letters*, *27*(16), 2513–2516. https://doi.org/10.1029/2000GL011438

Sherwood, S. C., Horinouchi, T., & Zeleznik, H. A. (2003). Convective impact on temperatures observed near the tropical tropopause. *Journal of the Atmospheric Sciences*, *60*(15), 1847–1856. https://doi.org/10.1175/1520-0469(2003)060<1847:CIOTON>2.0.CO;2

Sherwood, S. C., Roca, R., Weckwerth, T. M., & Andronova, N. G. (2010). Tropospheric water vapor, convection, and climate. *Reviews of Geophysics*, *48*(2), RG2001. https://doi.org/10.1029/2009rg000301

Smith, J. B., Wilmouth, D. M., Bedka, K. M., Bowman, K. P., Homeyer, C. R., Dykema, J. A., et al. (2017). A case study of convectively sourced water vapor observed in the overworld stratosphere over the United States. *Journal of Geophysical Research: Atmospheres*, *122*(17), 9529–9554. https://doi.org/10.1002/2017JD026831

Solomon, S., Rosenlof, K., Portmann, R., Daniel, J., Davis, S., Sanford, T., & Plattner, G.-K. (2010). Contributions of stratospheric water vapor changes to decadal variations in the rate of global warming. *Science*, *327*(5970), 1219–1223. https://doi.org/10.1126/science.1182488

Tan, J., Jakob, C., Rossow, W. B., & Tselioudis, G. (2015). Increases in tropical rainfall driven by changes in frequency of organized deep convection. *Nature*, *519*(7544), 451–454. https://doi.org/10.1038/nature14339

Tegtmeier, S., Anstey, J., Davis, S., Dragani, R., Harada, Y., Ivanviu, I., et al. (2020). Temperature and tropopause characteristics from reanalyses data in the tropical tropopause layer. *Atmospheric Chemistry and Physics*, *20*(2), 753–770. https://doi.org/10.5194/acp-20-753-2020

Ueyama, R., Jensen, E. J., & Pfister, L. (2018). Convective influence on the humidity and clouds in the tropical tropopause layer. *Journal of Geophysical Research: Atmospheres*, *123*(14), 7576–7593. https://doi.org/10.1029/2018JD028674

Ueyama, R., Jensen, E. J., Pfister, L., Diskin, G. S., Bui, T. P., & Dean-Day, J. M. (2014). Dehydration in the tropical tropopause layer: A case study for model evaluation using aircraft observations. *Journal of Geophysical Research: Atmospheres*, *119*(9), 5299–5316. https://doi.org/10.1002/2013JD021381

Ueyama, R., Jensen, E. J., Pfister, L., & Kim, J.-E. (2015). Dynamical, convective, and microphysical control on wintertime distributions of water vapor and clouds in the tropical tropopause layer. *Journal of Geophysical Research: Atmospheres*, *120*(19), 10483–10500. https://doi.org/10.1002/2015JD023318

Ueyama, R., Jensen, E. J., Pfister, L., Krämer, M., Afchine, A., & Schoeberl, M. (2020). Impact of convectively detrained ice crystals on the humidity of the tropical tropopause layer in boreal winter. *Journal of Geophysical Research: Atmospheres*, *125*(14), e2020JD032894. https://doi.org/10.1029/2020JD032894

Virts, K., Wallace, J. M., Fu, Q., & Ackerman, T. P. (2010). Tropical tropopause transition layer cirrus as represented by CALIPSO lidar observations. *Journal of the Atmospheric Sciences*, *67*(10), 3097–3112. https://doi.org/10.1175/2010JAS3413.1

Wang, P. K. (2003). Moisture plumes above thunderstorm anvils and their contributions to cross-tropopause transport of water vapor in midlatitudes. *Journal of Geophysical Research*, *108*(D6), 4194. https://doi.org/10.1029/2002JD002581

Wang, X., Dessler, A. E., Schoeberl, M. R., Yu, W., & Wang, T. (2019). Impact of convectively lofted ice on the seasonal cycle of water vapor in the tropical tropopause layer. *Atmospheric Chemistry and Physics*, *19*(23), 14621–14636. https://doi.org/10.5194/acp-19-14621-2019

Wofsy, S. C., McConnell, J. C., & McElroy, M. B. (1972). Atmospheric $CH_4$, CO, and $CO_2$. *Journal of Geophysical Research*, *77*(24), 4477–4493. https://doi.org/10.1029/JC077i024p04477

Yulaeva, E., Holton, J. R., & Wallace, J. M. (1994). On the cause of the annual cycle in tropical lower-stratospheric temperatures. *Journal of the Atmospheric Sciences*, *51*(2), 169–174. https://doi.org/10.1175/1520-0469(1994)051<0169:OTCOTA>2.0.CO;2